DEMONSTRATION REPORT

Advanced EMI Models for Live-site UXO Discrimination at Former Camp Beale

ESTCP Project MR-201101

FEBRUARY 2012

Fridon Shubitidze
Sky Research, Inc.

ESTCP

Report Documentation Page

Form Approved
OMB No. 0704-0188

1. REPORT DATE	2. REPORT TYPE	3. DATES COVERED
FEB 2012		**00-00-2012 to 00-00-2012**

4. TITLE AND SUBTITLE	5a. CONTRACT NUMBER
Advanced EMI Models for Live-site UXO Discrimination at Former Camp Beale	5b. GRANT NUMBER
	5c. PROGRAM ELEMENT NUMBER
6. AUTHOR(S)	5d. PROJECT NUMBER
	5e. TASK NUMBER
	5f. WORK UNIT NUMBER
7. PERFORMING ORGANIZATION NAME(S) AND ADDRESS(ES) **Sky Research, Inc,445 Dead Indian Memorial Road,Ashland,OR,97520**	8. PERFORMING ORGANIZATION REPORT NUMBER
9. SPONSORING/MONITORING AGENCY NAME(S) AND ADDRESS(ES)	10. SPONSOR/MONITOR'S ACRONYM(S)
	11. SPONSOR/MONITOR'S REPORT NUMBER(S)

12. DISTRIBUTION/AVAILABILITY STATEMENT
Approved for public release; distribution unlimited

13. SUPPLEMENTARY NOTES

14. ABSTRACT

15. SUBJECT TERMS

16. SECURITY CLASSIFICATION OF:			17. LIMITATION OF ABSTRACT	18. NUMBER OF PAGES	19a. NAME OF RESPONSIBLE PERSON
a. REPORT	b. ABSTRACT	c. THIS PAGE			
unclassified	**unclassified**	**unclassified**	**Same as Report (SAR)**	**55**	

Table of Contents

List of Figures

List of Tables

List of Acronyms

AIC	Akaike Information Criterion
APG	Aberdeen Proving Ground
BIC	Bayesian Information Criterion
BUD	Berkeley UXO Discriminator
cm	Centimeter
DLL	Dynamic Link Libraries
DoD	Department of Defense
EM	Electromagnetic
EMA	Expectation Maximization Algorithm
EMI	Electromagnetic Induction
ESTCP	Environmental Security Technology Certification Program
FCS	Former Camp Sibert
GSEA	Generalized standardized excitation approach
IDA	Institute for Defense Analyses.
ISO	Industry Standard Object
JD	Joint Diagonalization
MEG	Magneto encephalographic
ML	Maximum Likelihood
μs	Microsecond
mm	Millimeter
MM	MetalMapper
MPV	Man-Portable Vector
ms	Millisecond
MR	Munitions response
MSR	Multi-static response
MUSIC	Multiple Signal Classification
NC	North Carolina
NSMS	Normalized surface magnetic source
NV/SMS	Normalized volume or surface magnetic source models
ONVMS	Orthogonal normalized volume magnetic source
ONV/SMS	Orthonormalized volume or surface magnetic source models
PNN	Probabilistic Neural Network
ROC	Receiver Operating Characteristic
SERDP	Strategic Environmental Research and Development Program
SLO	San Luis Obispo
SVM	Support vector machine
TD	Time Domain
TEMTADS	Time Domain Electromagnetic Towed Array Detection System
TOI	Target of Interest
UXO	Unexploded Ordnance

1 INTRODUCTION

This demonstration report is designed to illustrate the discrimination performance at an actual UXO live-site of a set of advanced models for the analysis and inversion of electromagnetic induction (EMI) data that go far beyond the popular but often inadequate simple dipole scheme. The suite of methods, which combines the orthonormalized volume magnetic source (ONVMS) model, a data-preprocessing technique based on joint diagonalization (JD), and differential evolution (DE) minimization, among others, was tested at the former Camp Beale in California. The partially wooded site is contaminated with a mix of 37-mm, 60-mm, 81-mm, and 105-mm munitions, as well as complete and partial fuzes. For brevity we abstain from repeating demonstration- and site-specific information already presented elsewhere; the interested reader may turn to the ESTCP Live Site Demonstration Plan [1] and similar documents for enlightenment on these topics.

1.1 Background

The Environmental Security Technology Certification Program (ESTCP) recently launched a series of live-site UXO blind tests taking place in increasingly challenging and complex sites [1],[2]. The first classification study was conducted in 2007 at the UXO live-site at the former Camp Sibert in Alabama using two commercially available first-generation EMI sensors (the EM61-MK2 and the EM-63, both from Geonics). At this site, the discrimination test was relatively simple: one had to discriminate large intact 4.2″ mortars from smaller range scrap, shrapnel and cultural debris, and the anomalies were very well separated.

The second ESTCP discrimination study took place in 2009 at the live-UXO site at Camp San Luis Obispo (SLO) in California and featured a more challenging topography and a wider mix of targets of interest (TOI) [2]. Magnetometers and first-generation EMI sensors (again the Geonics EM61-MK2) were deployed on the site and used in survey mode for a first screening. Afterwards, two advanced EMI sensing systems—the Berkeley UXO Discriminator (BUD) and the Naval Research Laboratory's TEMTADS array—were used to perform cued interrogation of a number of the anomalies detected. A third advanced system, the Geometrics MetalMapper, was used in both survey and cued modes for anomaly identification and classification. Among the munitions buried at SLO were 60-mm, 81-mm, and 4.2″ mortars and 2.36″ rockets; three additional types of munitions were discovered during the course of the demonstration.

The third site chosen was the former Camp Butner in North Carolina. This demonstration was designed to investigate evolving classification methodologies at a site contaminated with small UXO targets, such as 37-mm projectiles.

The next site to be chosen for an ESTCP blind test was the former Camp Beale, whose roughly 60,000 acres straddle Yuba and Nevada Counties in California [1]. The demonstration was conducted in a 10-acre area located within the historical bombing and the Toss Bomb target area using several advanced EMI sensors, both handheld (MPV-II and 2×2-3D TEMTADS) and cart-based (MetalMapper). The site was selected because it is partially wooded and because it contains a wide mixture of TOI (including ISO, 37-mm, 60-mm, 81-mm, and 105-mm UXO) and fuzes and fuze parts that could be considered TOI on some sites. These two features, plus the magnetically responding soils encountered at the camp, are common occurrences in production

sites and add yet another layer of complexity into the classification process, providing additional opportunities to demonstrate the capabilities and limitations of the advanced EMI models at performing classification under a variety of site conditions.

1.2 Brief site history

Please refer to the ESTCP Live Site Demonstration Plan [1].

1.3 Objective of the demonstration

The advanced EMI models used for the analysis were developed under SERDP Project MM-1572 and used with great success in the previous ESTCP tests [2],[4],[5],[6] and on data collected at the Aberdeen Proving Ground (APG) in Maryland. In order to improve and demonstrate the robustness and reliability of the models for live-site UXO discrimination, however, one must keep putting them to the test at progressively challenging sites and for an increasing number of next-generation EMI instruments sensors. The principal objectives of this project are thus to apply advanced EMI models to UXO discrimination on actual live sites and to demonstrate their classification capability in real-world scenarios. The specific technical objectives are to:

1. Demonstrate the discrimination capability of the advanced EMI models for live-site conditions;
2. Invert for target intrinsic parameters and use these to identify robust classification features that may help distinguish UXO from non-hazardous objects; in other words, the technology should
    a. Indentify all seeded and native UXO;
    b. Discard at least 75% of non-TOI targets;
3. Indentify sources of uncertainty in the classification process and incorporate them into the dig/no-dig decision process;
4. Understand and document the applicability and limitations of the advanced EMI discrimination technologies in the context of project objectives, site characteristics, and suspected ordnance contamination.

2 TECHNOLOGY

The advanced EMI models and statistical signal processing approaches developed and tested over the past three years under SERDP Project MM-1572 were able to detect and identify buried UXO ranging in caliber from 25 mm up to 155 mm. The technique was seen to be physically complete, fast, accurate, and clutter-tolerant, and provided excellent classification in both single- and multiple-target scenarios when combined with multi-axis/transmitter/receiver sensors like TEMTADS and the MetalMapper [3]. The methodology, augmented to include a suite of classifiers, was also adapted to handheld sensors like the MPV and the 2 × 2-3D TEMTADS [7]. In this section we describe the different techniques one by one.

2.1 The orthonormalized volume magnetic source model

The advanced models we have developed for UXO discrimination include the normalized surface magnetic source (NSMS) model [28] and the orthonormalized volume magnetic source (ONVMS) model [13]. The NSMS procedure can be considered as a generalized surface dipole model: in it, an object's response to a sensor is modeled mathematically using a set of equivalent pointlike analytic solutions of the Maxwell equations (usually dipoles, though charges are also a possibility) distributed over a surface surrounding the object. The amplitudes of the sources are proportional to the component of the primary magnetic field normal to the surface; once this dependence is normalized out, the NSMS strengths can be determined directly by solving a linear system of equations that results from minimizing the mismatch between measured and modeled data for a known object-sensor combination.

The ONVMS model, a further extension of NSMS, posits that the entire scatterer can be replaced with a set of magnetic dipole sources distributed over a computational volume. We make the usual EMI assumptions: we neglect displacement currents and electric fields and conduction currents in air and soil. The primary magnetic field established by the sensor penetrates the objects in its vicinity to some degree, inducing eddy currents and magnetic dipoles inside them which in turn produce a secondary or scattered magnetic field. This is the field that we propose to represent as due to a volumetric distribution of magnetic dipole density:

$$\mathbf{H}^{\mathrm{sc}}(\mathbf{r}, p) = \int_V \frac{1}{4\pi R^3}(3\hat{\mathbf{R}}\hat{\mathbf{R}} - \bar{\bar{\mathbf{I}}}) \cdot \mathbf{m}(\mathbf{r}_v', p) dv' = \int_V \bar{\bar{G}}(\mathbf{r}, \mathbf{r}') \cdot \mathbf{m}(\mathbf{r}_v', p)\, dv', \tag{1}$$

where $p = \{t, f\}$ is time or frequency, $\hat{\mathbf{R}}$ is the unit vector along $\mathbf{R} = \mathbf{r} - \mathbf{r}_v'$, $\mathbf{r}_v'$ is the position of the v'-th infinitesimal dipole in the volume V, $\mathbf{r}$ is the observation point, and $\bar{\bar{\mathbf{I}}}$ and $\bar{\bar{G}}(\mathbf{r}, \mathbf{r}')$ are respectively the identity and Green dyads. The induced magnetic dipole moment $\mathbf{m}(\mathbf{r}_{v'}, p)$ at point $\mathbf{r}_{v'}$ on the surface is related to the primary field through $\mathbf{m}(\mathbf{r}_{v'}, p) = \bar{\bar{\mathbf{M}}}(\mathbf{r}_{v'}, p) \cdot \mathbf{H}^{\mathrm{pr}}(\mathbf{r}_{v'})$, where $\bar{\bar{\mathbf{M}}}(\mathbf{r}_{v'}, p)$ is the symmetric polarizability tensor. The secondary magnetic field at any point can be expanded in a set of orthonormal functions $\bar{\bar{\psi}}_i(\mathbf{r})$ as

$$\mathbf{H}(\mathbf{r}) = \sum_{i=1}^{N_v} \bar{\bar{\psi}}_i(\mathbf{R}_i) \cdot \mathbf{b}_i \,, \tag{2}$$

where we have also introduced the expansion coefficients $\mathbf{b}_i$. The $\bar{\bar{\psi}}_i$ are linear combinations of dipole Green dyads guaranteed to be orthonormal by the Gram–Schmidt process; thanks to this property the amplitudes of the tensor elements of $\bar{\bar{\mathbf{M}}}_i(p)$ can be determined without having to solve a linear system of equations. The great advantages of ONVMS are that it takes into account the mutual couplings between different sections of the targets and that it avoids matrix singularity problems in multi-object cases. It treats single- and multi-target scenarios on the same footing. Once the tensor elements and locations of the responding dipoles are determined one can group them within the volume and for each group calculate the total polarizability, which at the end is joint-diagonalized. These diagonal elements have been shown to be intrinsic to the objects, and can be used, either on their own or in combination with other quantities, in discrimination processing [6].

2.2 Joint diagonalization for data preprocessing

EMI sensors currently feature multi-axis illumination of targets and tri-axial vector sensing, or exploit multi-static array data acquisition [1]–[6]. To take advantage of the rich data sets that these sensors provide, we recently developed and successfully demonstrated a discrimination procedure based on joint diagonalization [15]. To illustrate the application of JD to advanced EMI sensors, we proceed to describe its implementation for the MetalMapper [3]. The system consists of $K = 3$ mutually perpendicular transmitters and $M = 7$ triaxial receivers. The sensor activates the transmitter loops in sequence, one at a time, and for each transmitter all receivers measure the complete transient response over a wide dynamic range of time, approximately from 100 microseconds (μs) to 8 milliseconds (ms), over 45 time gates. The sensor thus provides 3×21 spatial data points for any given time channel t_q, $q = 1, 2, \ldots, N_q$, where N_q is the number of the time channels. If we define $H_{k,m\{zyx\}}$ as the *z*, *y*, or *x*-component of the magnetic field measured by the *m*-th receiver coil when the *k*-th transmitter is active, then the $K \times 3M$ matrix

$$\bar{\bar{H}}(t_q) = \begin{bmatrix} H_{1,1z} & H_{1,1y} & H_{1,1x} & \cdots & H_{1,7z} & H_{1,7y} & H_{1,7x} \\ H_{2,1z} & H_{2,1y} & H_{2,1x} & \cdots & H_{2,7z} & H_{2,7y} & H_{2,7x} \\ H_{3,1z} & H_{3,1y} & H_{3,1x} & \cdots & H_{3,7z} & H_{3,7y} & H_{3,7x} \end{bmatrix} \tag{3}$$

will be a set of measured data vectors for the *k*-th transmitter for each time channel. One can then construct a new matrix $\bar{\bar{B}}(t_q) = \bar{\bar{H}}^T(t_q)\, \bar{\bar{H}}(t_q)$ again for each time channel, and, through an eigen-decomposition, express it in terms of a diagonal matrix $\bar{\bar{D}}(t_q)$ of eigenvalues and an orthogonal matrix $\bar{\bar{U}}(t_q)$ of eigenvectors:

$$\bar{\bar{B}}(t_q) = \bar{\bar{U}}(t_q)\, \bar{\bar{D}}(t_q)\, \bar{\bar{U}}^T(t_q)\,, \tag{4}$$

where *T* denotes the transpose. In order to relate the time-dependent eigenvalues to the number of potential targets we find a *single* set $\bar{\bar{V}}$ of eigenvectors that will be shared by all $\{\bar{\bar{B}}(t_q)\}_{q=1}^{N_q}$ matrices and will also make all their off-diagonal elements as vanishingly small as possible:

$$\left\{\bar{\bar{D}}(t_q)\right\}_{q=1}^{N_q} = \bar{\bar{V}}^T \left\{\bar{\bar{B}}(t_q)\right\}_{q=1}^{N_q} \bar{\bar{V}}. \quad (5)$$

The technique that finds an orthogonal (*i.e.*, real and unitary) matrix $\bar{\bar{V}}$ that minimizes the $\{\bar{\bar{B}}(t_q)\}_{q=1}^{N_q}$ matrices' off-diagonal elements is called "joint diagonalization" (JD) [15]. The diagonal matrices $\{\bar{\bar{D}}(t_q)\}_{q=1}^{N_q}$ contain information about the targets that contribute to the signal. Our studies show that each set of three above-threshold diagonal elements of the measured multi-static response (MSR) data matrix describe one target. We have also demonstrated that the JD technique is a robust technique for extracting target signals in cases with a low signal-to-noise-ratio. In addition, the eigenvalues' time dependence exhibits the different targets' classification features [14].

2.3 EMI Data inversion: A global optimization technique

Determining a buried object's orientation and location is a non-linear problem. Inverse-scattering problems are solved by determining an objective function [14] as a goodness-of-fit measure between modeled and measured magnetic field data. Standard gradient search approaches often suffer from a surfeit of local minima that sometimes result in incorrect estimates for location and orientation. To avoid this problem we recently developed a different class of global optimization search algorithms. One such technique is the Differential Evolution (DE) method [26]–[27], a heuristic, parallel, direct-search method for minimizing non-linear functions of continuous variables that is very easy to implement and has good convergence properties. We combined DE with ONVMS to invert digital geophysical EMI data [6]. All EMI optimizations were split into linear and nonlinear parts, iterating between them to minimize the objective function. Once the target locations are found, the amplitudes of responding ONVMS are determined and used to classify the object relative to items of interest.

2.3.1 Discrimination parameters

To classify targets in this demonstration we used ONVMS combined with DE optimization and joint diagonalization to invert for the locations of the targets of interest (TOI). The model provides at least three independent total ONVMS parameters along the principal axis for each potential target that can be used for discrimination. During the inversion stage the total time-dependent ONVMS, which depends on the size, geometry, and material composition of the object in question, is determined for each potential target. Early time gates bring out the high-frequency response to the shutdown of the exciting field; the induced eddy currents in this range are superficial, and a large total ONVMS amplitude at early times correlates with large objects and large surface area. At late times, when the eddy currents have diffused completely into the object and low-frequency harmonics dominate, the EMI response relates to the metal content (i.e., the volume) of the target. Thus a smaller but compact object has a relatively weak early response that dies down slowly, while a large but thin or hollow object has a strong initial

response that decays quickly. These parameters can be used to form feature vectors for classification.

The success of classification depends on the selection of features, the separation of different classes in feature space, and the ability of the sensor data to constrain the estimated features. In some cases, due to poor signal-to-noise ratio, the feature vectors from UXO targets can be corrupted or could be similar with clutter anomalies. In such cases, we must recognize that discrimination may be limited or classification decision will require an override using an expert's judgment. When discrimination is possible we use both template-matching and statistical procedures—such as Gaussian Mixture models, support vector machines (SVM) [17], or probabilistic neural networks (PNN) [22]—since no single classifier is likely to be applicable under all conditions [16].

2.3.2 Clustering of CBE anomalies

The distribution of power-law/exponential-decay parameters extracted from the total ONVMS profiles is key to performing classification. This is because TOI with similar total ONVMS are likely to show similar patterns under various conditions. By comparing the total ONVMS time-decay parameters of unknown targets to those of known objects one can predict the class/cluster to which the unknown targets belong. There are many clustering techniques available, such as K-means [18], Principal Component Analysis [24], and Support Vector Machines [16].

2.3.3 Classification using template matching

The template matching technique is a classification approach that discriminates unknown targets from TOI by comparing the extracted target's features—in our case the total ONVMS—to a set stored in library. There are two ways to execute the template-matching technique: 1) using code that will estimate least-square mismatches between the unknown and library targets ONVMS, and 2) by visual inspection. Since in the case of Camp Beale there were unexpected TOI (whole and partial fuzes), we used both approaches when classifying the targets.

2.4 Details of classification schemes

The discrimination process comprises three sequential tasks: data collection, data inversion, and classification. Each EMI sensor produces unique data sets and therefore requires its own data inversion and classification schemes. This section summarizes the data inversion and classification schemes for the MetalMapper, the 2×2-3D TEMTADS array, and the MPV sensor.

2.4.1 MetalMapper data inversion and classification scheme

The MM sensor's Tx and Rx signals detailed modeling approach using the ONVMS-DE algorithm is described in [14].

Step 1. Data pre-processing: All MM-data were pre-processed using a Matlab Code (see Appendix 9.3). The code reads comma-delimited format CSV files and transfers them to ASCII files compatible with the ONVMS-DE code (ONVMS_MM.exe). The user needs only specify the path to the folder with the CSV files; the code then converts them all.

Step 2. Create MM MSR data matrix: Using equation (3) we construct the measurement matrix $\bar{\bar{H}}(t_q)$ for each anomaly and use it to create the MM MSR matrix $\bar{\bar{B}}(t_q) = \bar{\bar{H}}^T(t_q)\,\bar{\bar{H}}(t_q)$.

Step 3. Eigenvalue analysis: The JD technique is applied to the created MM MSR data matrix to extract the time-dependent eigenvalues for each anomaly. The eigenvalues for some of the Camp Beale anomalies are depicted in Figure 1 and Figure 2. The MSR data matrix eigenvalues are intrinsic properties of the targets; each target has at least three eigenvalues above the threshold (noise level: low magnitude eigenvalues). For example, Figure 2 shows the eigenvalues extracted for a) a 105-mm projectile and a 81-mm mortar, (center row) a 60mm mortar and a 37-mm munition, and (third row) an ISO target, and a fuze part. The results in Figure 2 illustrate that each target has distinguishable eigenvalues that can be used for classification; Note that the magnitudes of the MSR eigenvalues depend on the depths and orientations of the targets [14]; therefore the user should use only their shapes when performing classification. As the number of targets increases (as in the first row of Figure 1), so does the number of eigenvalues above the noise level. The MSR matrix can also help in assessing the quality of the data: as the signal-to-noise ratio (SNR) decreases the eigenvalues for the targets and the ground exhibit similar behaviors (see the second row of Figure 1). For Beale MM classification, we examined the eigenvalues versus time for each case and used them to estimate the number of targets and SNR. We used this information to build a custom training list. For the most part, the custom training list based on the JD analysis contained anomalies that had too many above-threshold and small eigenvalues, like the samples depicted in Figure 1. Once we had the estimated number of targets and SNR for each anomalies we proceeded to invert all cued MM datasets using the combined ONVMS-DE algorithm for multi-targets.

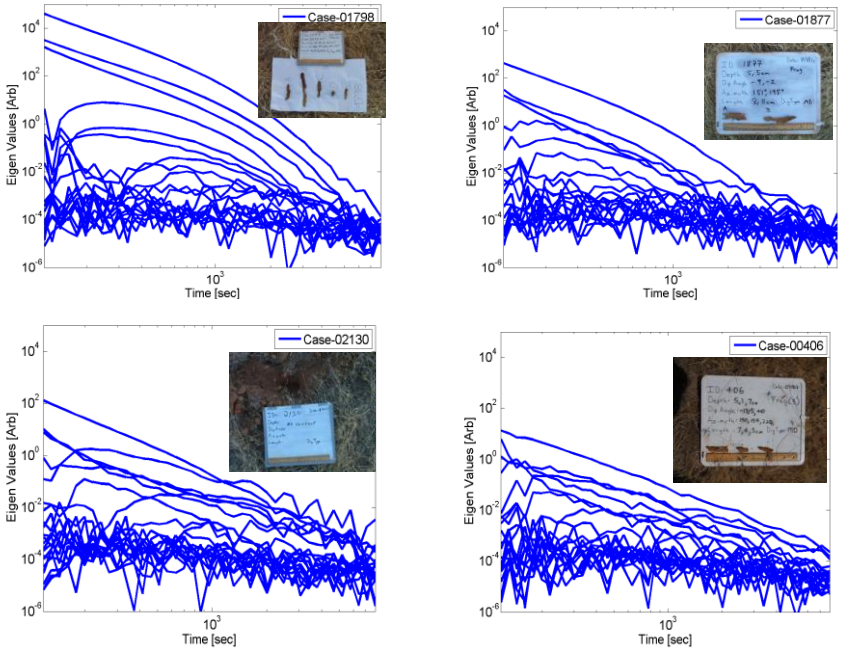

Figure 1. Camp Beale MM multi-static response matrix eigenvalues versus time for some samples of requested anomalies.

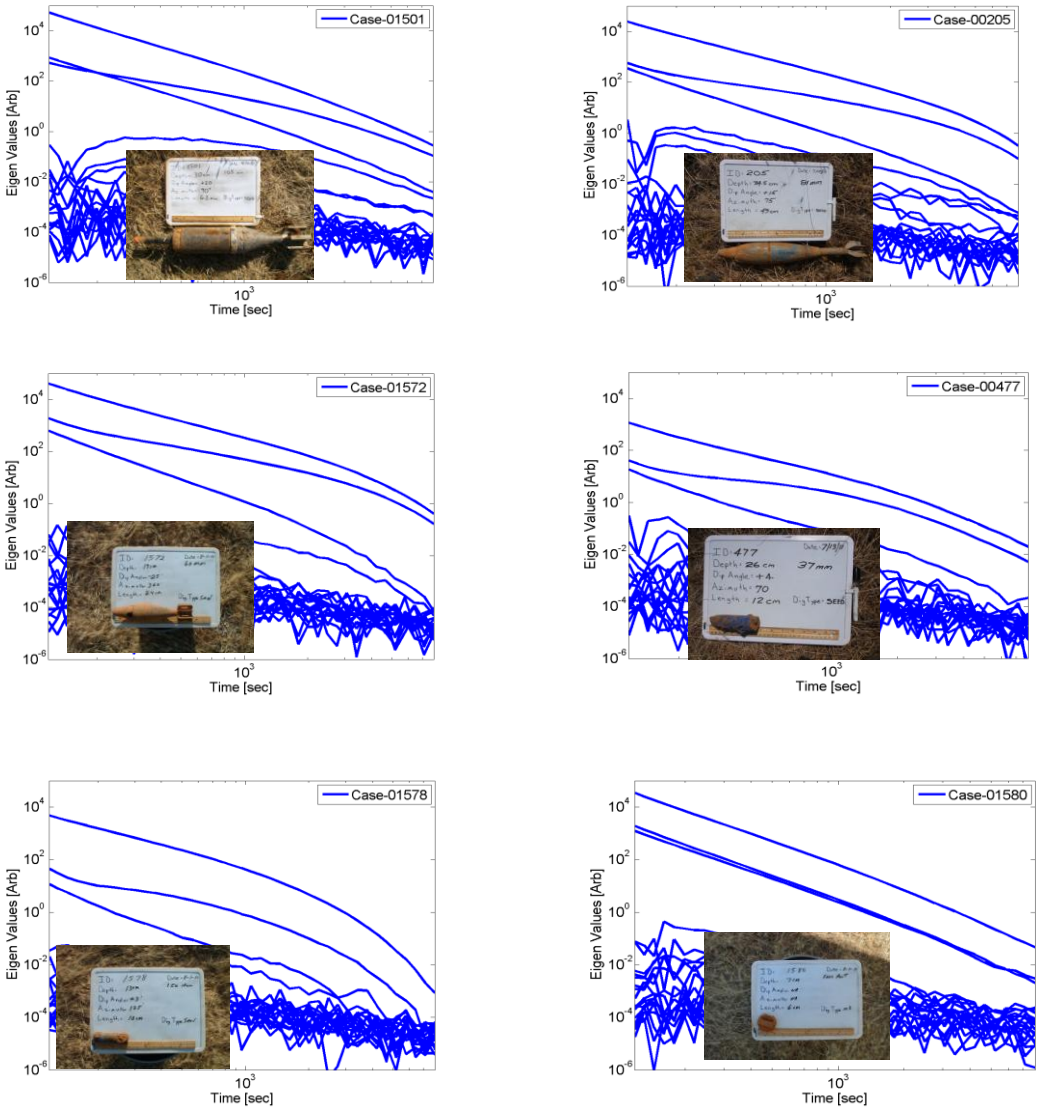

Figure 2. MM multi-static response matrix eigenvalues versus time for (top row) a 105-mm projectile and an 81-mm mortar, (center row) a 60mm mortar and a 37-mm munition, and (third row) an ISO target, and a fuze part.

Step 4. Extract the total ONVMS for each anomaly. We ran a Matlab code (given in Appendix 9.4) to extract the targets' extrinsic and intrinsic parameters, including the total ONVMS as shown in Figure 3.

Step 5. Create a custom training list. We use the size (the inverted ONVMS at the first time channel) and decay (ratio of the inverted total ONVMS at the *n*-th time channel to that at the first) as parameters; see Figure 4. The values of $\log_{10}[M_{zz}(t_1)/M_{zz}(t_n)]$ versus $\log_{10}[M_{zz}(t_1)]$ are plotted in for all Camp Butner MM data sets, at the 5th, 10th, 20th, and 35th time channels. Visual examination shows that there are no distinguishable clusters at the 5th channel; at later times, on the other hand, the decay-vs.-size distribution starts to cluster. We used the features evaluated at the 35th time channel and applied statistical classification

techniques. The Matlab code that uses the inverted ONVMS for clustering is given in Appendix 9.5; it also uses Matlab's built-in function "clusterdata". In this studies the size ($\log_{10}(\text{TONVMS}_{zz}(t_1))$) and decay ($\log_{10}(\text{TONVMS}_{zz}(t_1) / \text{TONVMS}_{zz}(t_n))$) parameters for $n = 35$ are used for clustering and the number of clusters is 8% of the total number of anomalies. For each cluster we computed the centroid and determined the anomaly closest to it. This anomaly we included in the custom training data list (see the Matlab code in Appendix 9.5). The clustering results are depicted in Figure 5. Each color corresponds to a cluster; circles denote anomalies for which the ground truth was asked. In addition to the statistical clustering algorithm, ONVMS time decay curves were inspected for each anomaly: we used the TONVMS time decay shapes and symmetries to further validate or modify the custom training anomaly list. Anomalies with significantly asymmetric TONVMS were removed from the training list; anomalies with fast decay but symmetric profiles were added to the training list for which we requested the identifying ground truth. Some samples of such anomalies are shown in Figure 6.

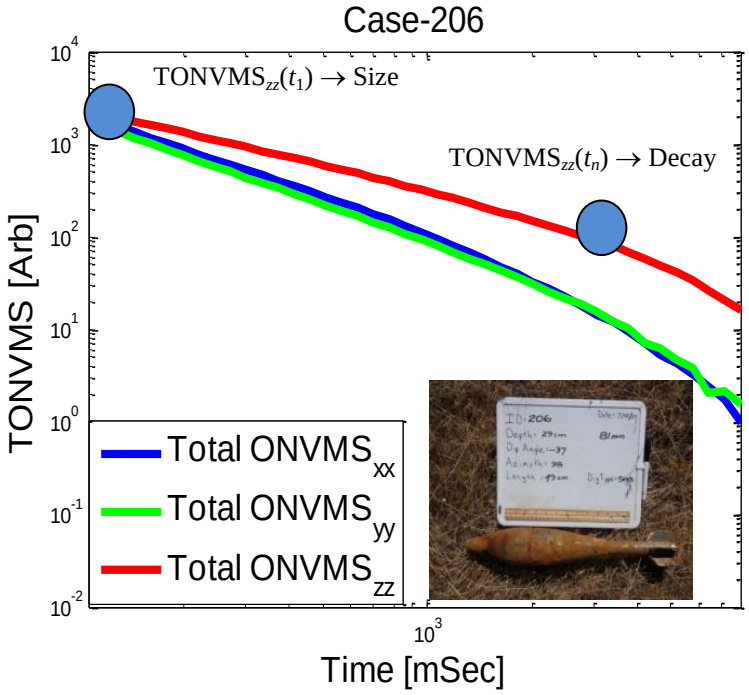

Figure 3. Inverted total ONVMS time-decay profiles for an 81-mm mortar in the camp Beale study, Anomaly #206.

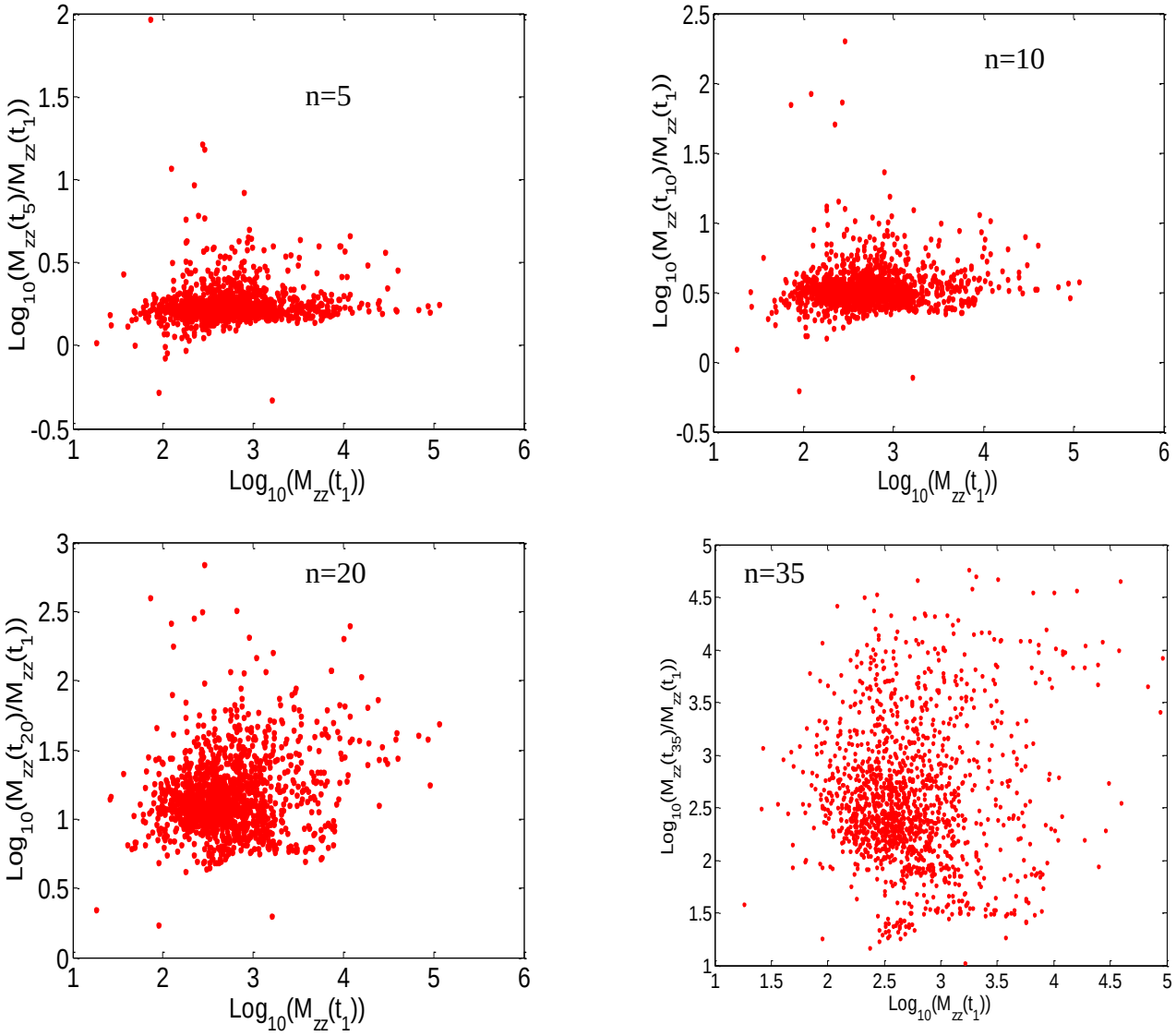

Figure 4. Scatter plot of size and decay for all Camp Beale MM anomalies based on the extracted total ONVMS for time channels Nos. 5, 10, 20, and 35.

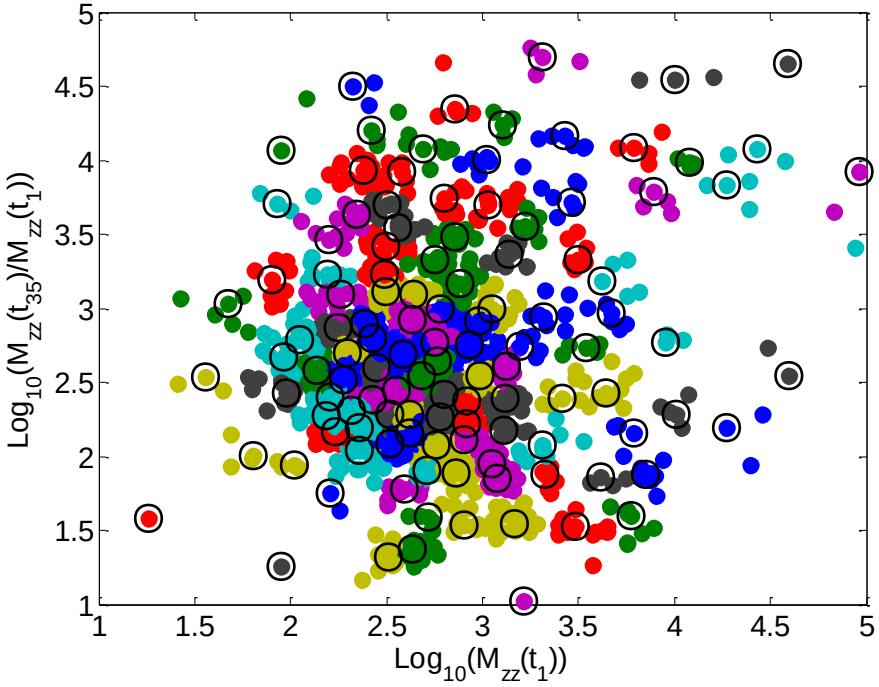

Figure 5. Result of the clustering for the Camp Beale MM anomalies using the size and shape information for $n = 35$ (Figure 4). The circles denote the anomalies for which the ground truth was asked.

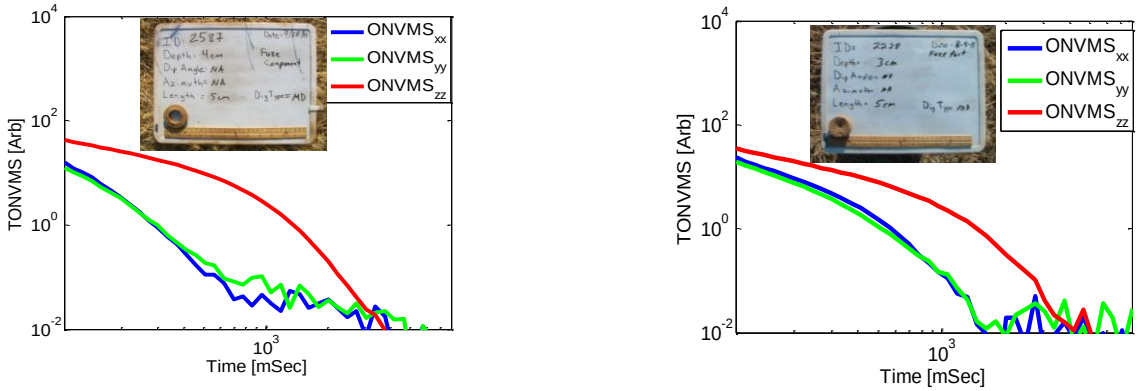

Figure 6. TONVMS vs. time for some samples of Camp Beale MM anomalies. In the delivered ground truth, Anomaly # 2228 was identified as a TOI.

Step 6. Request ground truth for selected anomalies; The custom training list, a combination of JD, clustering and ONVMS-DE single-target inversion results, was submitted to the ESTCP office, who then provided the ground truth for training. We used the delivered ground truth to identify the different possible TOI types and their size variations. There were native site-specific fuzes and fuze parts which the ESTCP office initially identified as TOI. We used this information to create a second list of training anomalies, based on total ONVMS curves

obtained using a multi-target inversion code, which we again submitted to ESTCP. The ground truth for the second list indicated that there were fuzes of varying size and material composition. We further examined the ONVMS-DE multi-target cases and produced a third anomaly list that was submitted to the ESTCP office.

Step 7. Create ranked dig list. Armed with the ground truth of custom identified training anomalies (a total of 132) and the inverted total ONVMS for each MM cued data we created a library for 105-mm, 81-mm, 60-mm, 37-mm, and ISO munitions, fuzes, and fuze parts. The inverted total ONVMS for the anomalies that were classified as TOI appear in Figure 7 and Figure 8. All the inverted total ONVMS are seen to cluster well, and each target has a total ONVMS with features—such as its amplitude at the first time channel, its decay rate, or the separation between the primary (red lines) and secondary/tertiary (blue/green) components at different time channels—that make it amenable to identification.

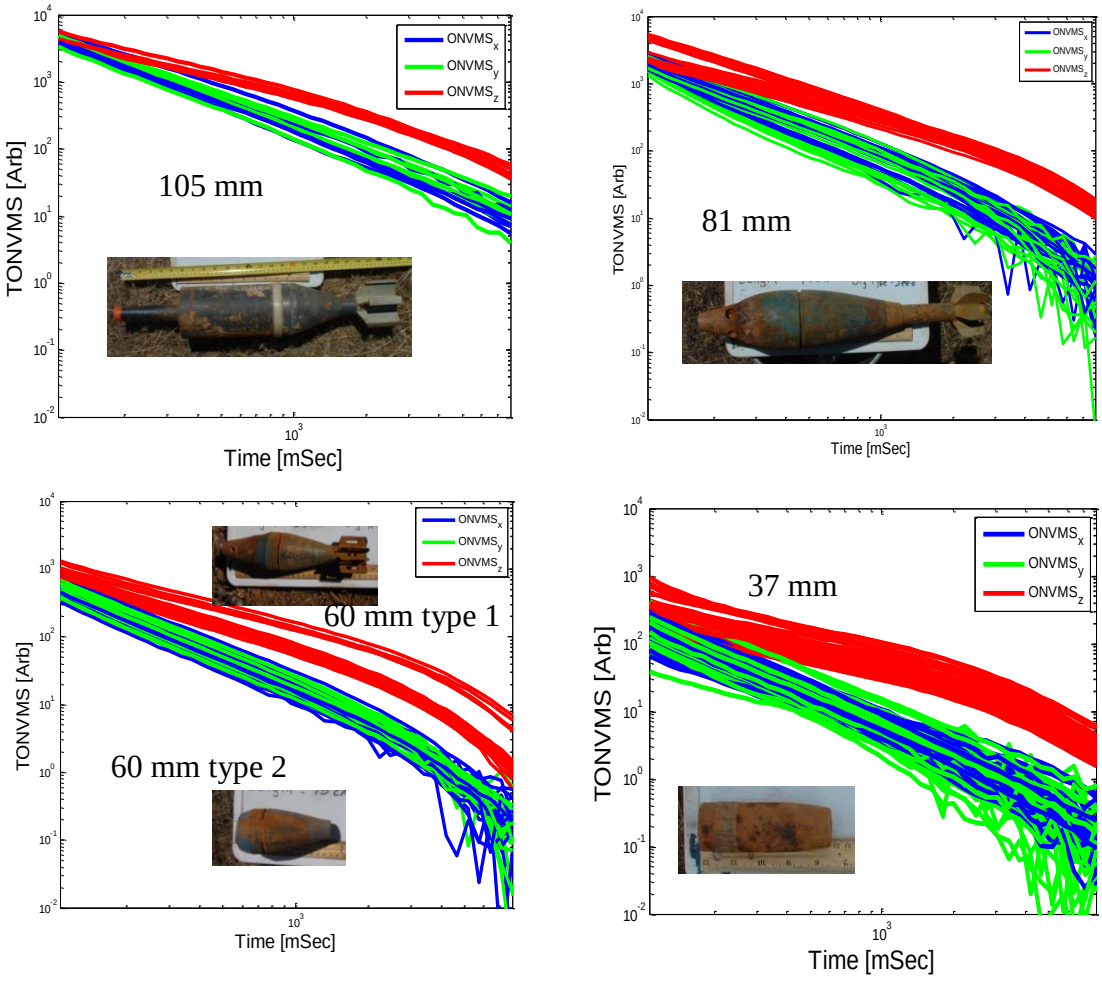

Figure 7. Inverted total ONVMS time-decay profiles for four targets: (top row) 105-mm projectile and 81-mm mortar, and (bottom) 60-mm mortar and 37-mm projectile.

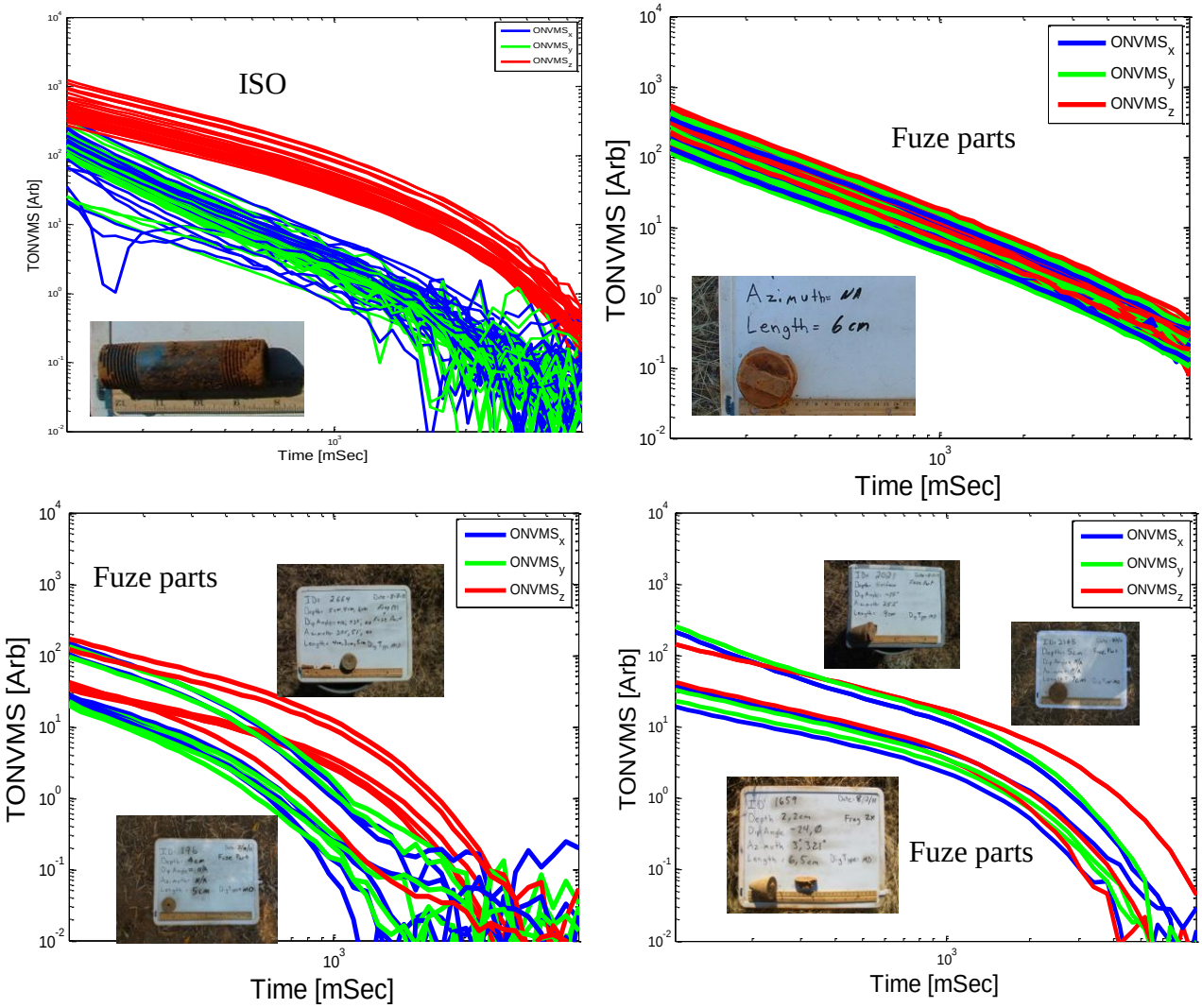

Figure 8. Inverted total ONSMS time decay profiles for ISO (excluded training ISOs) targets and fuze parts.

Step 8. Submit the dig list to ESTCP. There were two Camp Beale MM cued data sets collected by UXO production teams from Parsons and CH2MHILL. We processed both data sets independently. The CHM2HILL MM data were processed by the Sky Research R&D team using the classification procedure described above; the Parsons data were processed by the Sky Research production team using only the ONVMS library-matching technique. Independent final prioritized dig lists were created for both sets of data and submitted to the Institute for Defense Analyses (IDA) for independent scoring.

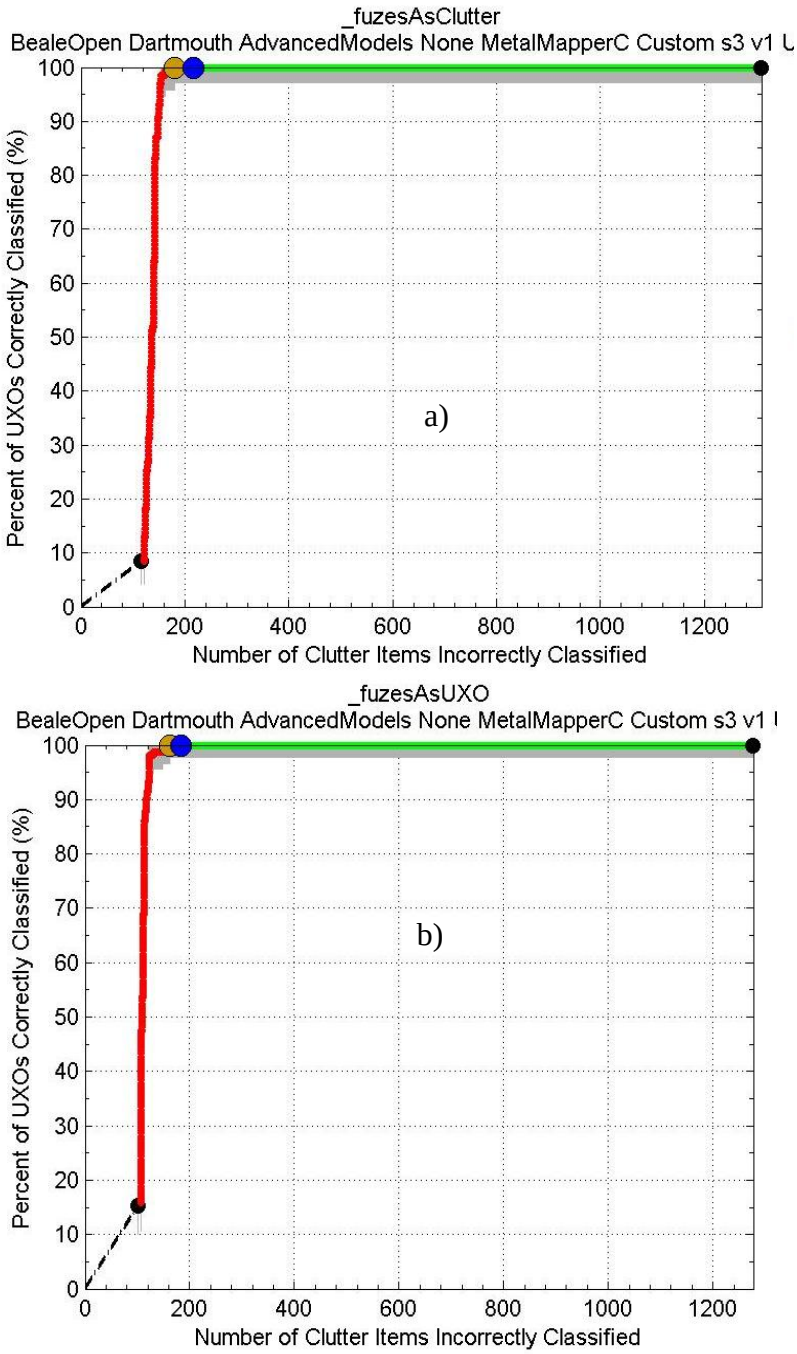

Figure 9. ROC curves for CH2MHILL Camp Beale MM data sets. The results were obtained by the Sky Research R&D team using library-matching and statistical classification approaches. In (a) it is assumed that fuzes are clutter; in (b) they are considered TOI.

a) Camp Beale CH2MHILL MM data classification results

The IDA scored results for CH2MHILL MM 1470 anomalies in the form of a receiver operating characteristic (ROC) curves are depicted in Figure 9 a) and Figure 9 b) assuming respectively that fuzes are clutter and that they are TOI. The result shows that a) of the 132 targets that were dug for training, 107 targets were not TOI (shift along *x*-axis) and 25 were (shift along *y*-axis); b) there are no false negatives: all 170, of which 89 were UXO/ISO and 33 were fuzes, TOI were correctly identified; c) to classify all TOI correctly only 65 extra (false positive) digs are needed; d) for increased classification confidence the algorithm requested an additional eleven digs after all TOI had been identified correctly, 1117 (~86 % of clutters out of 1300) were identified as non-TOI with high confidence.

b) Camp Beale Parsons MM Data classification results

The Sky Research production team first inverted total ONVMS for potential TOI using testing data collected at the site. They then visually compared the total ONVMS time-decay curves of potential targets to those of the test anomalies. During the comparisons "suspicious" targets were identified. The targets did not match any library targets yet exhibited UXO-like features, such as potential BOR symmetry and slow decays. The "suspicious" anomalies were included in a list of training anomalies whose ground truth was requested from the ESTCP office. The delivered ground truth revealed two unexpected TOI fuze types that were added to the library. Using the updated library, all targets were ranked as TOI and clutter; the dig list was created and submitted to the IDA office for scoring. The resulting ROC curves are depicted in Figure 10 a) and b) assuming fuzes to be respectively clutter and TOI. The result shows that a) of the 69 targets that were dug for training, 50 were not TOI (shift along *x*-axis) and 19 were (shift along *y*-axis); b) no false negatives: all TOI (a total of 170) were identified correctly; c) to classify all TOI correctly only 203 extra (false positive) digs are needed; d) 1047 (~81 % of clutter items) were identified as non-TOI with high confidence.

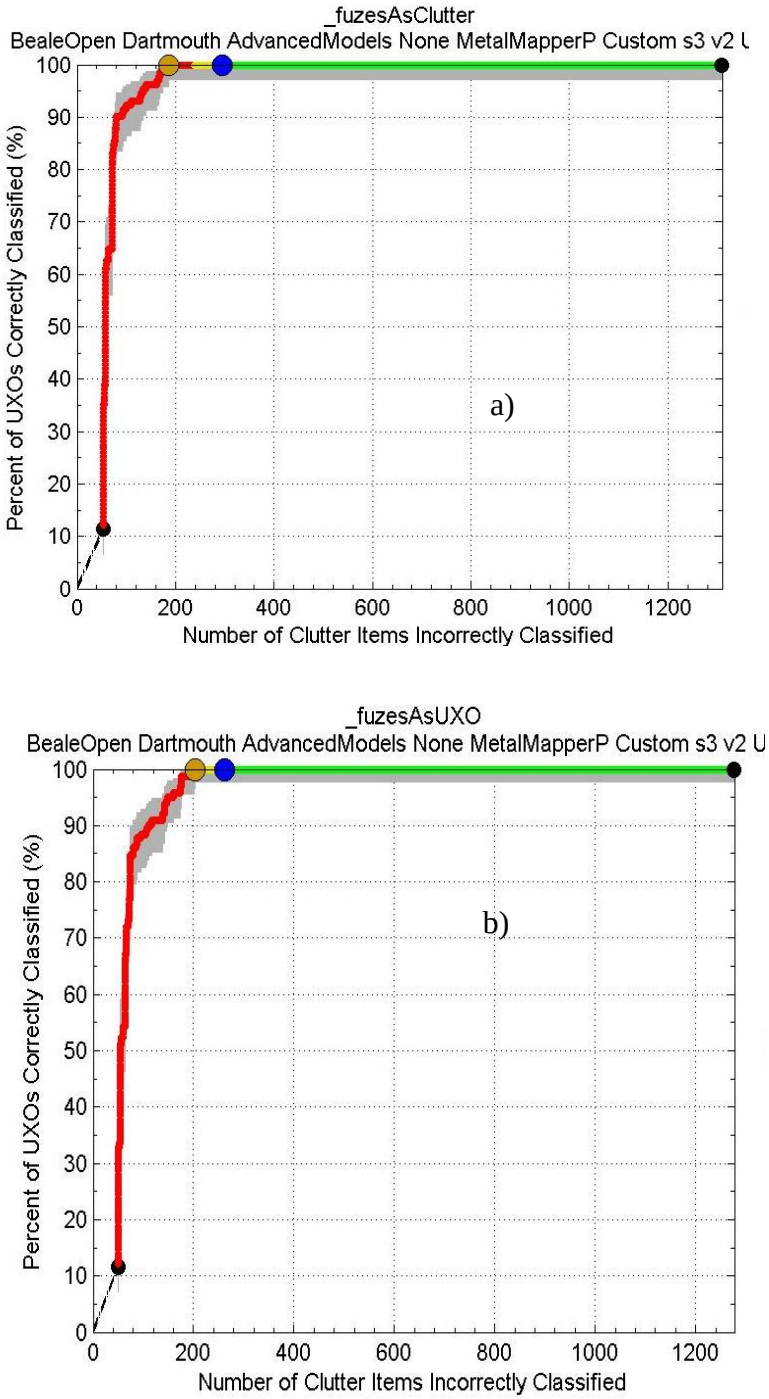

Figure 10. ROC curve for Parsons Camp Beale MM data sets. The results were obtained by the Sky Research production team using library-matching classification. In a) fuzes are considered clutter; in b) fuzes are assumed to be TOI.

2.4.2 2 × 2-3D-TEMTADS data sets data inversion and classification scheme

The 2 × 2 3D-TEMATDS area is a next-generation portable EMI system. The instrument's electronics, geometry, data collection procedure, and file formats are described in [6]. For the Camp Beale 2 × 2-3D TEMATDS cued data we applied the inversion and classification protocol described above for the MM data sets.

Step 1. Transfer all CSV files to an ASCII-based format compatible with the TEMATDS ONVMS-DE code (ONVMS_2_2.exe).

Step 2. Construct the 2 × 2 TEMATDS MSR data matrix as described for MM.

Step 3. Apply JD to 2 × 2 TEMATDS MSR data matrix; extract eigenvalues versus time; conduct eigenvalue analysis; determine data quality and number of potential targets in each cell. The 2 × 2 TEMTADS MRS data matrix eigenvalues versus time for some camp Beale anomalies are depicted in Figure 11 and Figure 12; featured are an ISO, a 37-mm, a 60-mm, a 81-mm, and magnetic soil.

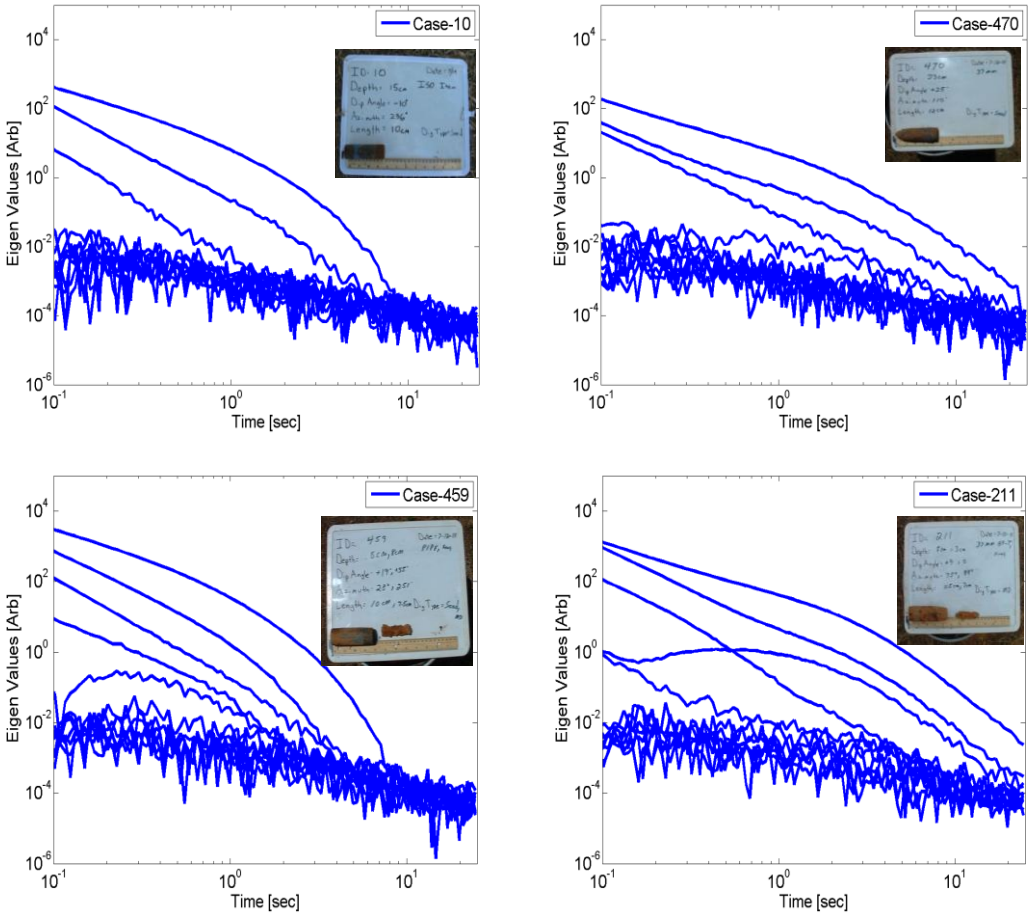

Figure 11. Camp Beale 2 × 2 MRS data matrix eigenvalues versus time for an ISO and a 37-mm; first row for single targets; the second row for two targets.

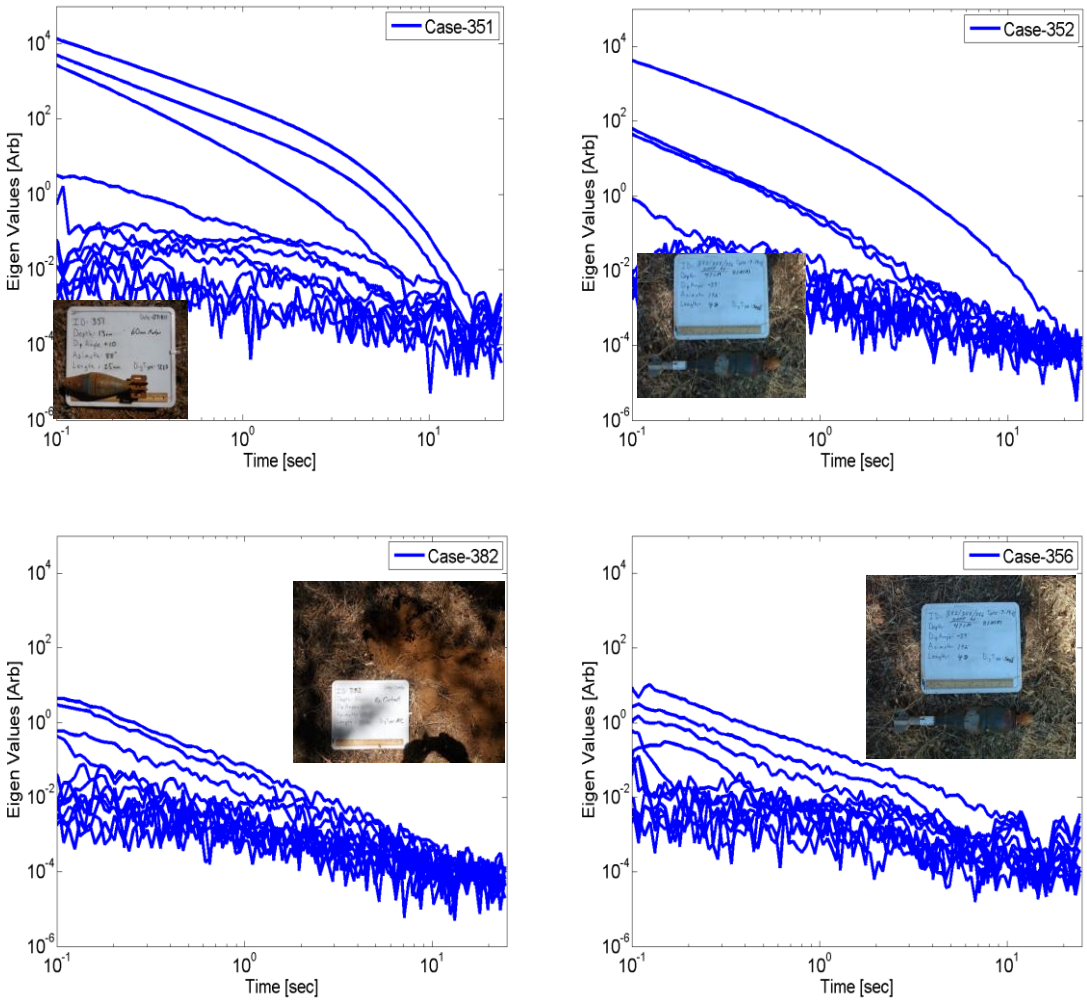

Figure 12. Camp Beale 2 × 2 MRS data matrix eigenvalues versus time for a 60-mm, an 81-mm, and magnetic soil.

The results show that the 2 × 2 TEMTADS MSR eigenvalues are intrinsic properties of the targets. Each target has very distinguishable eigenvalues that stay the same even when the signal is contaminated with signals from nearby targets (see Figure 11). We used the eigenvalues' characteristics directly to perform an initial classification. Figure 12 shows that the MRS data matrix eigenvalues provide fast and robust information about the data quality. For example, comparing Case-352 with Case-356 (Figure 12 second column) shows that when the sensor is well positioned above the target the eigenvalues are strong and well above the noise level; on the other hand, when the sensor is offset from the target the eigenvalues become noisy and mix with those of the soil (see Figure 12 for Case-382). In order to avoid misclassification, those anomalies were placed into the training data list. The results also indicate that as the number of targets increases, so does the number of eigenvalues above the noise level. The anomalies with a significant number of eigenvalues (> 6) above the noise level were also included in the training data; the 2 × 2 TEMATDS MSR eigenvalues for one such case are shown in Figure 13.

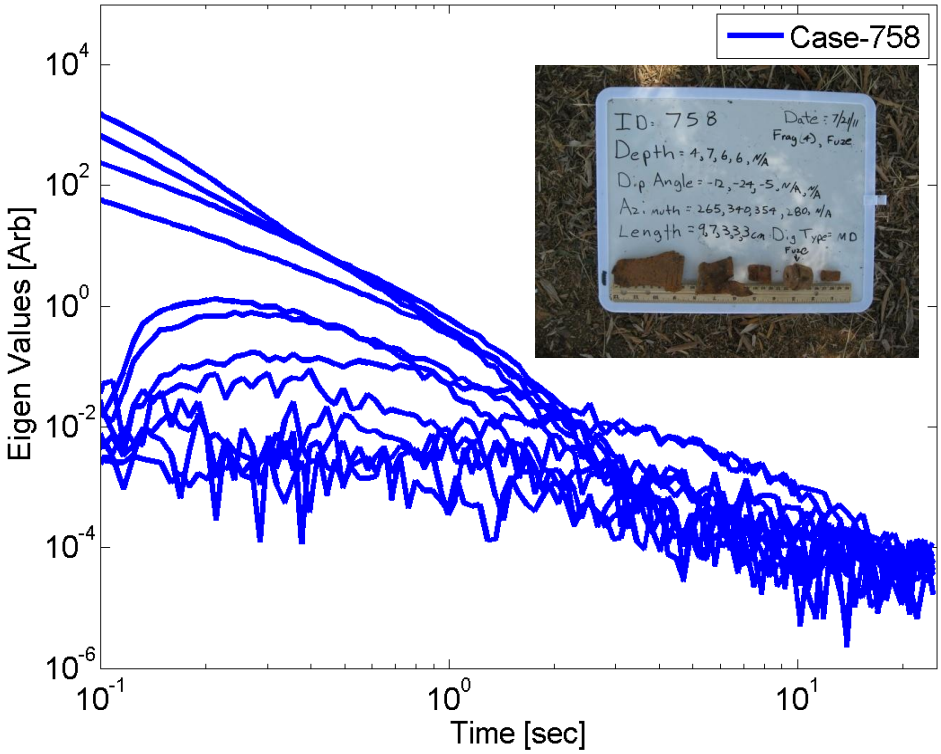

Figure 13. Camp Beale 2×2 TEMATDS MRS data matrix eigenvalues versus time for Test Case 758.

Figure 13 shows that there are no clear background-related eigenvalues (i.e., eigenvalues that have similar magnitude variations for all time channels), and there are at least seven distinguishable eigenvalues. For these two reasons we included the anomaly in the training data list. The received ground truth revealed that the cell had five targets, including a 3-cm fuze part that was ranked as a TOI by ESTCP.

Step 4. Extract the total ONVMS for each anomaly. We ran the Matlab code of Appendix 9.4 (replacing ONVMS_MM.EXE with ONVMS_2_2.EXE) and extracted the targets' intrinsic and extrinsic (attitude) parameters. The extracted total ONVMS for the 3-cm fuze part from Test Case-758 using a five-target inversion code is depicted in Figure 14. We see that the total ONVMS decays fast and is not symmetric, which could be explained by the signal contamination level. The ground truth shows that the signal is indeed contaminated significantly, since the TOI is smaller than the clutter and buried deeper. Even in these circumstances our model was able to extract meaningful parameters. This extracted ONVMS was then used to identify other similar fuze parts (seven in total).

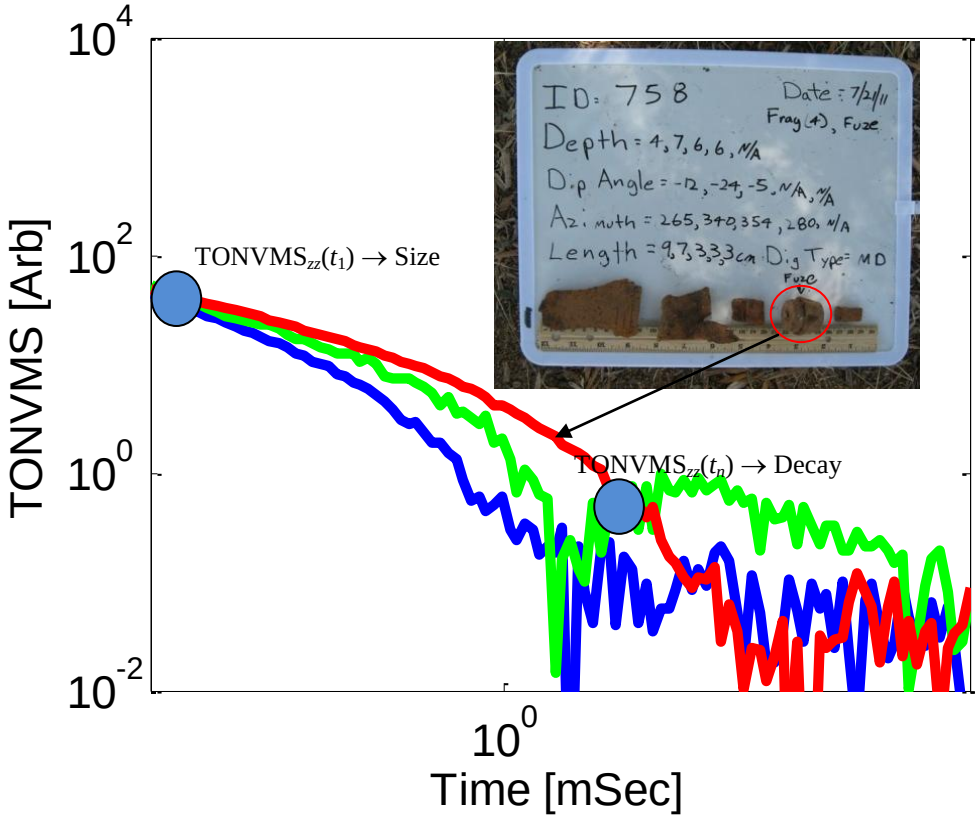

Figure 14. Total ONSMS for the 3-cm fuze part from Test Case-758 extracted using a five-target inversion code.

Step 5. Create a custom training list. To create the custom training list we used size and decay parameters (respectively the inverted ONVMS at the first time channel and the ratio of the inverted total ONVMS at the 80th time channel to that at the first; see Figure 14). Figure 15 is a scatter plot of $\log_{10}[M_{zz}(t_1)/M_{zz}(t_{80})]$ vs. $\log_{10}[M_{zz}(t_1)]$ for the data set. To cluster the anomalies we applied statistical classification to the size and decay distributions using the Matlab code of Appendix 9.5. The clustering results appear in Figure 16, where each color/circle corresponds to a cluster. In addition, we inspected the eigenvalues and ONVMS time decay curves for each anomaly to further validate or override the custom training anomaly list.

Step 6. Request ground truth for selected anomalies; We created a custom training list using a combination of JD, clustering, and ONVMS-DE inversion results. The list was submitted to the ESTCP office and the ground truth for training anomalies was received. Again we used the ground truth to identify the possible TOI types and their size variations, which information we then used to generate a second list of training anomalies.

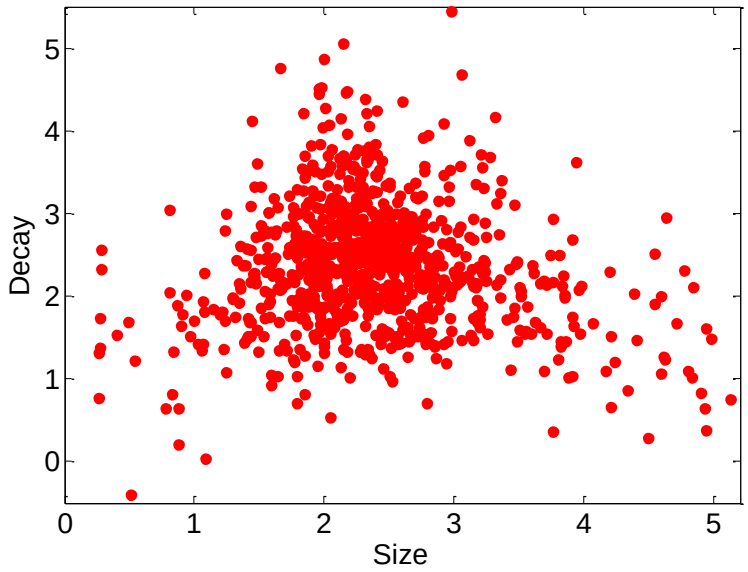

Figure 15. Scatter plot of size ($\log_{10}[\mathrm{TONVMS}_{zz}(t_1)]$) and decay ($\log_{10}[\mathrm{TONVMS}_{zz}(t_1)/\mathrm{TONVMS}_{zz}(t_{80})]$) for all Camp Beale 2 × 2 TEMTADS anomalies based on the extracted total ONVMS.

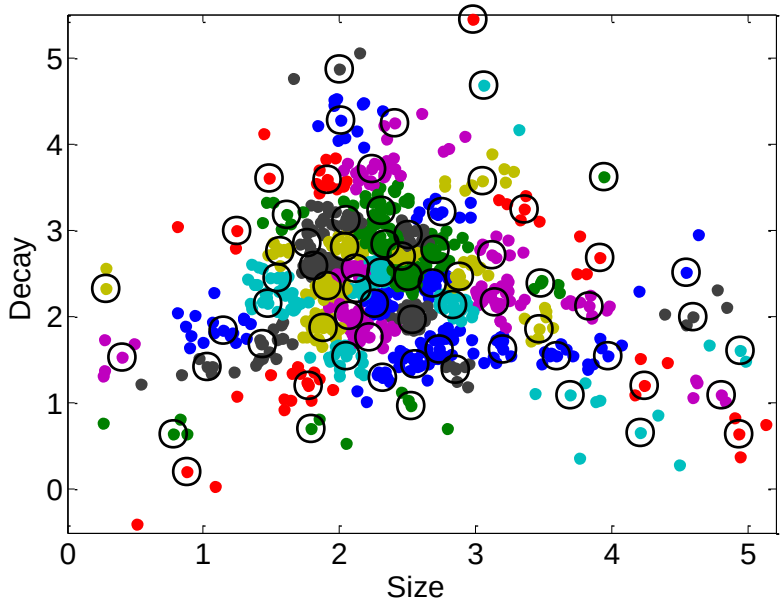

Figure 16. Result of the supervised clustering classification for the Camp Beale 2 × 2 TEMTADS anomalies using the size and shape information Figure 15.

Step 7. Create a ranked dig list. Using the ground truth from the previous step (98 anomalies in total) and the inverted total ONVMS for each 2 × 2 TEMTADS data file we created a library for 105-mm, 81-mm, 60-mm, 37-mm, and ISO munitions, fuzes, and fuze parts. The inverted total ONVMS for the anomalies that were classified as TOI appear in Figure 17, Figure 18, and Figure 19.

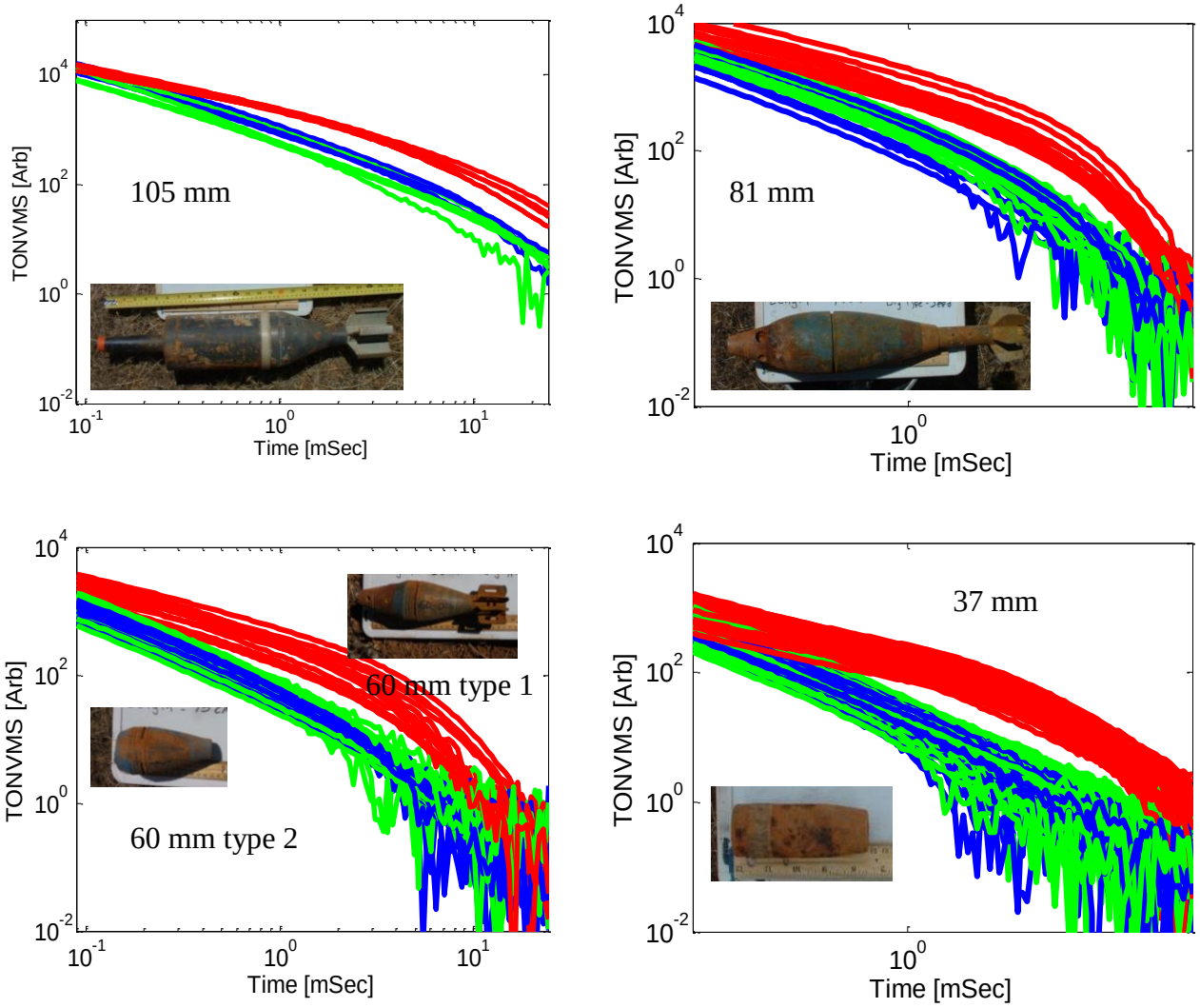

Figure 17. Total ONVMS versus time decay for Camp Beale 2 × 2 TEMATDS 105-mm, 81-mm, 60-mm and 37-mm TOI.

Step 8. Submit the dig list to ESTCP. We used the clustering and library-matching techniques to classify anomalies as containing TOI or not and submitted the resulting ranked list to the IDA for scoring; The scored results are for the 911 TEMTADS anomalies shown on Figure 20 (a) and (b), which respectively assume the fuze parts to be clutter and TOI. Of the 99 targets that were dug for training, 75 were not TOI (shift along *x*-axis) and 24 were (shift along *y*-axis). There were no false negatives: all TOI (a total of 124, of which 89 were UXO/ISO and 35 were fuzes) were classified correctly. To classify all TOI correctly, an extra 116 (false positive) digs were needed; d) 596 (~76% of 787 clutter items) were identified as non-TOI with high confidence.

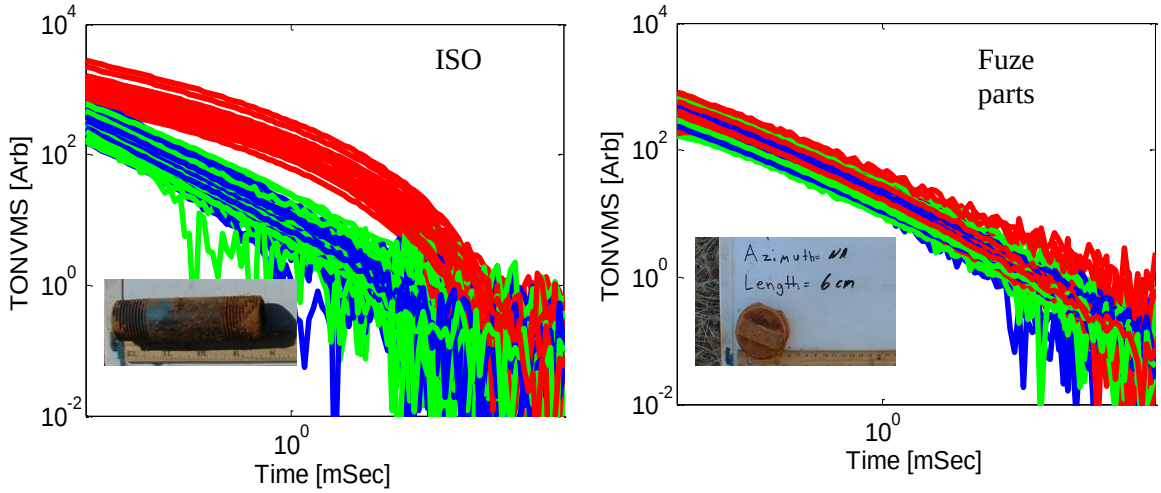

Figure 18. Total ONVMS versus time decay for Camp Beale 2×2 TEMATDS ISO and fuze parts.

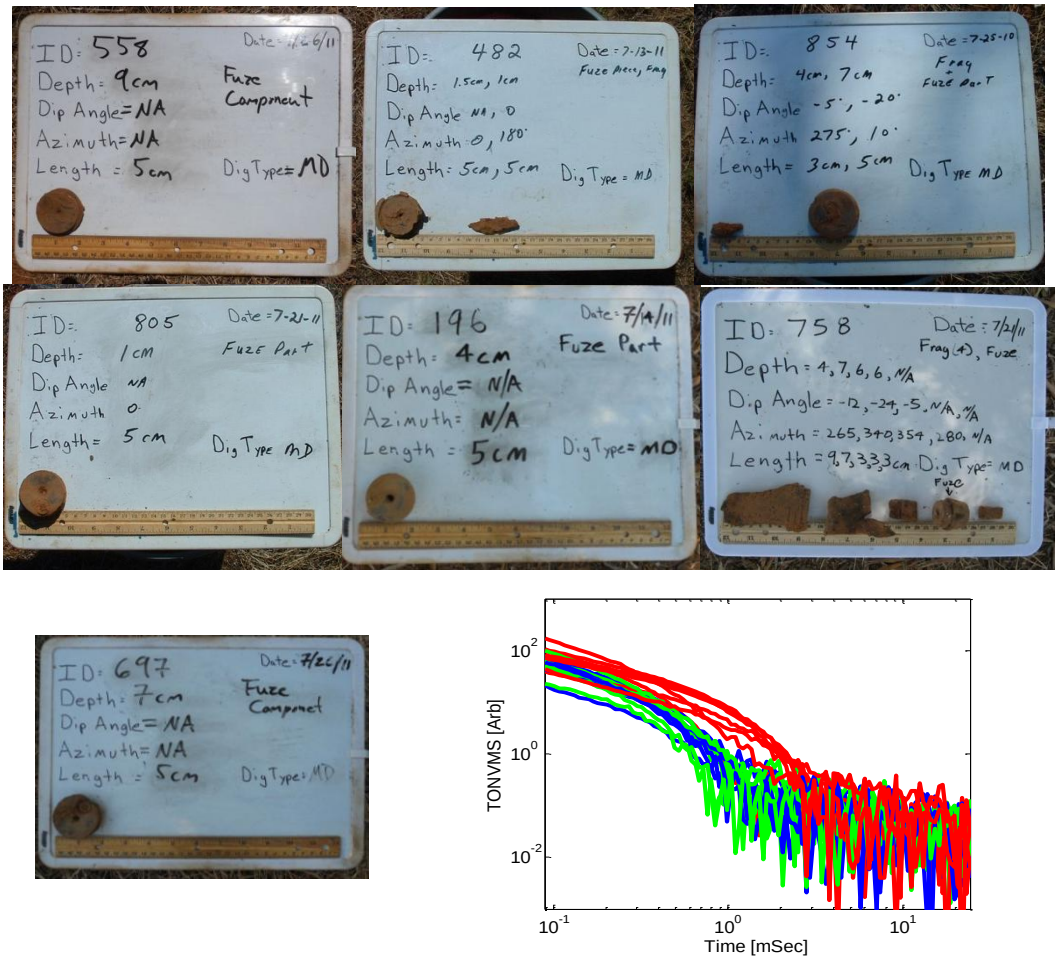

Figure 19. Images of seven small fuze parts that were identified as TOI by the ESTCP office. The bottom-right panel has the inverted total ONVMS for all these seven small fuze parts.

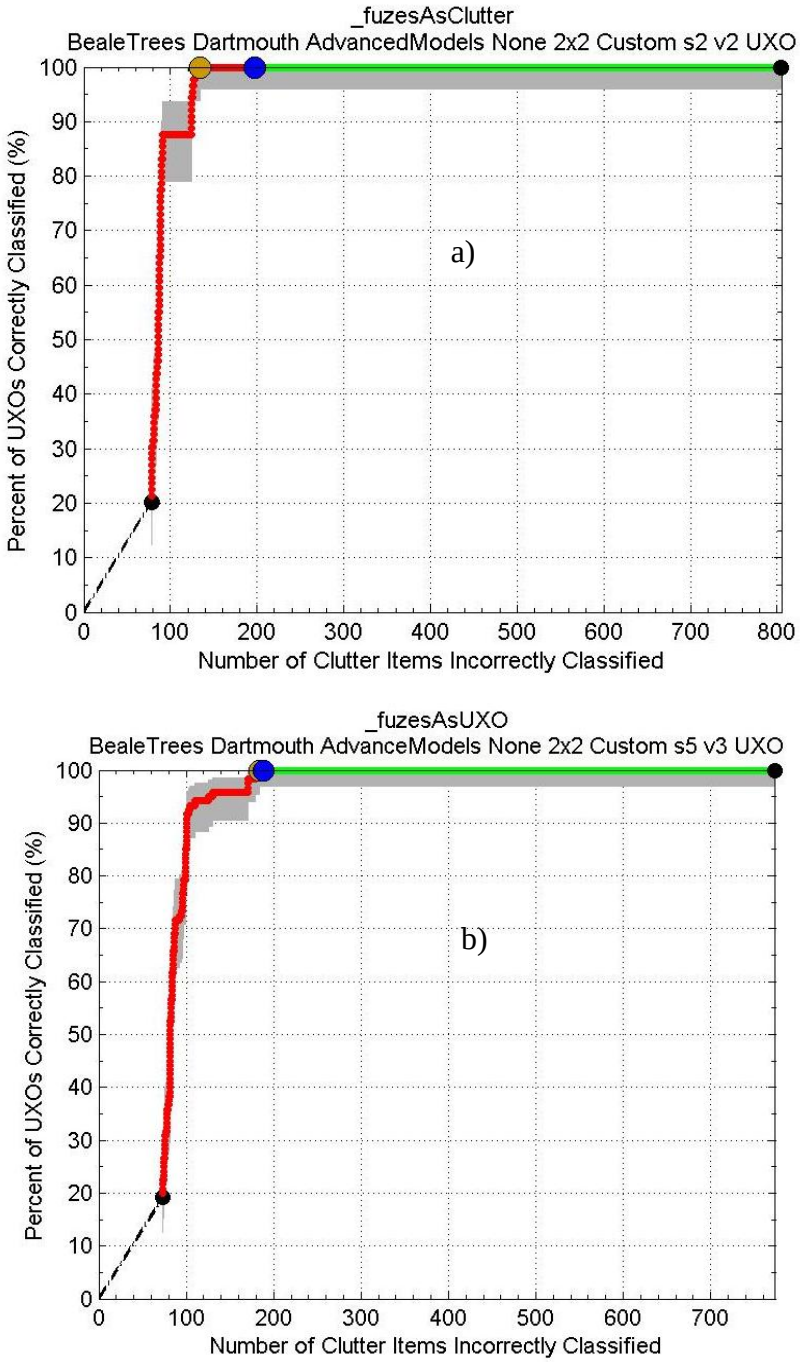

Figure 20. Camp Beale 2 × 2 TEMATDS anomalies ROC curve: a) fuzes as clutters; b) fuzes as TOI.

2.4.3 MPV-II data inversion and classification scheme

The man portable vector MPV-II is an advanced handheld EMI system, originally developed by ERDC-CRREL, G&G Sciences, and Dartmouth College under SERDP Project 1443. The advanced EMI models have been adapted to this instrument [14] and tested with various lab and

test-site data sets. The inversion and classification analysis of the Camp Beale MPV-II cued data was done following the same steps enumerated above:

Step 1. Extract total ONVMS for each anomaly. We ran the Matlab code from Appendix 9.4 (replacing ONVMS_MM.EXE with ONVMS_MPV.EXE) to extract target parameters;

Step 2. Create a custom training list: We used size and decay parameters (taking the 25th time channel for the latter) as inputs to the statistical classification technique that clustered the anomalies using the Matlab code of Appendix 9.5.

Step 3. Request ground truth for selected anomalies. We created a custom training list using combination of clustering and ONVMS-DE inversion results. The list was submitted to the ESTCP office and the ground truth for training anomalies was received.

Step 4. Create ranked dig list. Using the ground truth of custom identified training anomalies (a total of 95) and the inverted total ONVMS for each case we created a library for the different munitions, fuzes, and fuze parts. The inverted total ONVMS for the anomalies that were classified as TOI appear in Figure 21 and Figure 22.

Step 5. Submit the dig list to ESTCP. Using the clustering and library-matching techniques we classified the anomalies as TOI or non-TOI. The ranked list was submitted to the IDA for scoring; the results are shown on Figure 23 (a) and (b), which respectively assume the fuze parts to be clutter and TOI.

The scored results for the 911 Camp Beale MPV-TD anomalies, depicted in Figure 20, show that a) of the 95 targets that were dug for training, 79 were not TOI (shift along *x*-axis) and 16 were TOI (shift along *y*-axis); b) no false negatives: all TOI (124, of which 89 were UXO/ISO and 35 were fuzes) were classified correctly; c) to classify all TOI correctly one needed 121 extra (false positive) digs; d) 587 (~75 % of clutter items out of 787) were identified as non-TOI with high confidence.

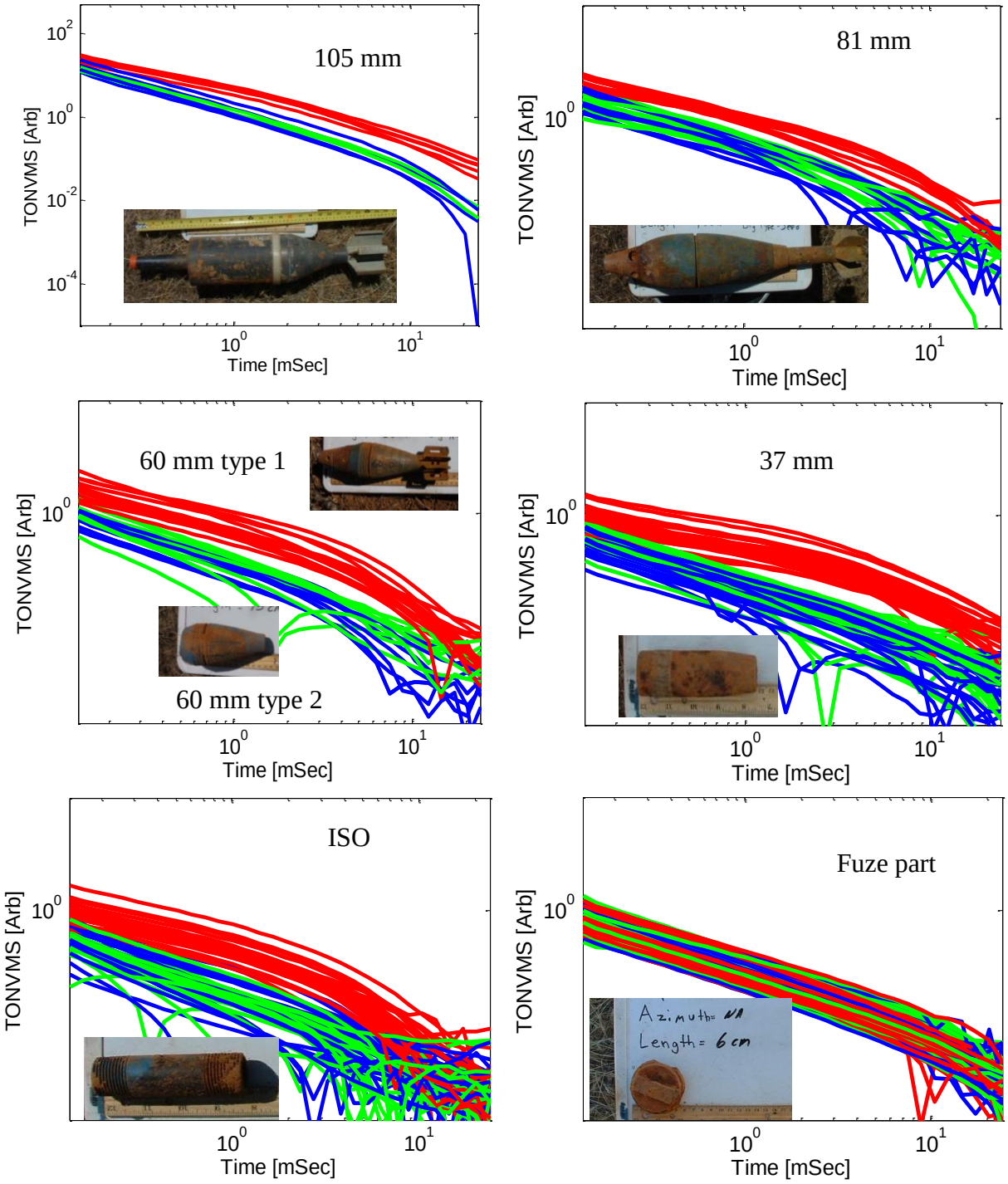

Figure 21. Total ONVMS versus time for Camp Beale MPV-TD 105-mm, 81-mm, 60-mm 37-mm, and ISO munitions and for the fuze parts identified as TOI by ESTCP.

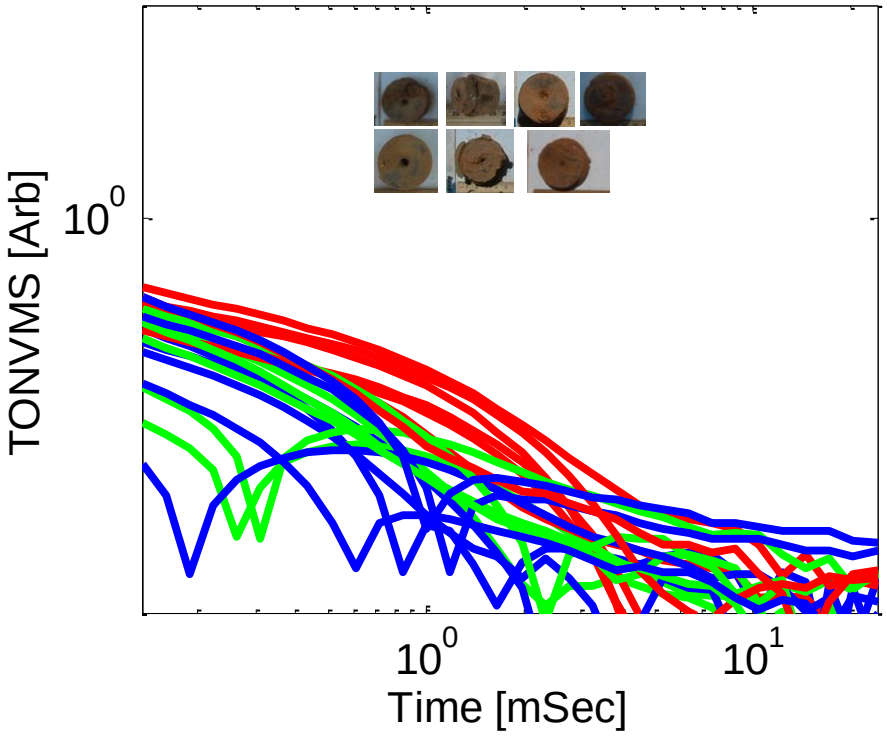

Figure 22. Inverted total ONVMS versus time for some of the small fuze parts identified as TOI by the ESTCP office.

2.5 Brief chronological summary

The basic concepts of the advanced EMI models have evolved largely from methodologies developed over the past 11 years by the Electromagnetic Sensing Group led by Dr. Fridon Shubitidze at Dartmouth College in close collaboration with researchers from ERDC-CRREL. The developments were supported by various SERDP projects. In 2007, SERDP awarded Project MM-1572, "A Complex Approach to UXO Discrimination: Combining Advanced EMI Forward and Statistical Signal Processing" to Sky Research, which supported the development and implementation of the NSMS model and several statistical classification algorithms (neural networks, support vector machines, and Gaussian mixture clustering among them). These methods were tested at APG, Camp Sibert, and SLO. The NSMS method was extended further to become the ONVMS technique. This model and the JD preprocessing technique were developed under the following SERDP projects: "Electromagnetic Induction Modeling for UXO Detection and Discrimination Underwater/Multi Target Inversion and Discrimination" (MM-1632, Dartmouth College), "Isolating and Discriminating Overlapping Signatures in Cluttered Environments", (MM-1664, a joint project between Dartmouth College and USACE-CRREL). Both ONVMS and JD were tested at the Camp Butner live site under SERDP MM-1572. *The project received a Project-of-the-Year award at the annual Partners in Environmental Technology Technical Symposium & Workshop held between November 29 and December 1st, 2011, in Washington, DC.*

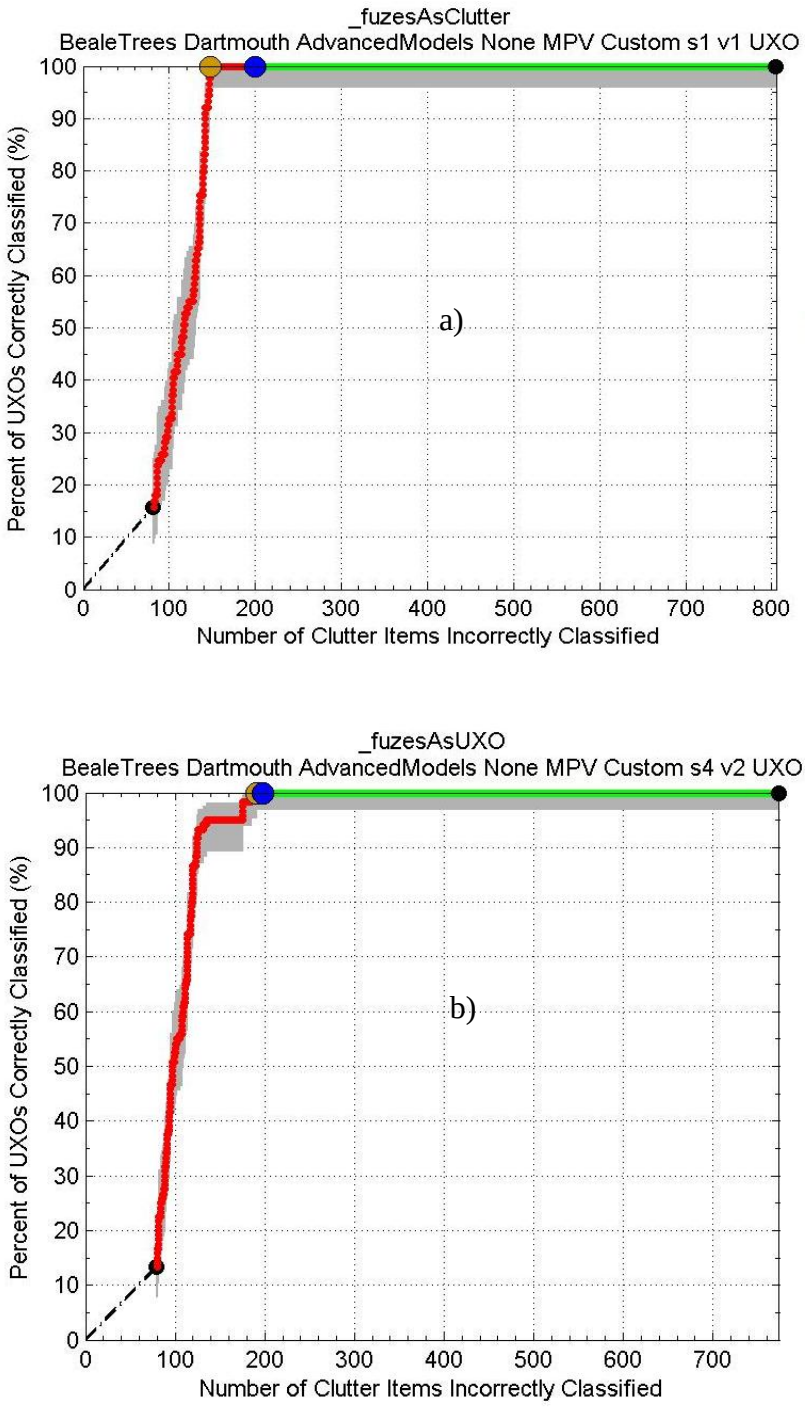

Figure 23. ROC for Camp Beale MPV-TD anomalies, a) assuming fuzes as clutter and b) considering fuzes to be TOI.

3 PERFORMANCE OBJECTIVES

The performance objectives of this ESTCP live site discrimination study were: to achieve high probability of discrimination of UXO from among a wide spread of clutter; to process all data sets; to minimize the number of data that could not be analyzed or decided upon; to minimize the number of false positives; and to identify all UXO with high confidence. The performance objectives are summarized in Table 1.

Table 1: Performance objectives

Performance Objective	Metric	Data Required	Success Criteria
Maximize correct classification of munitions	Number of targets of interest retained	• Prioritized anomaly lists • Scoring reports from the Institute for Defense Analyses (IDA)	The approach correctly classifies all targets of interest
Maximize correct classification of non-munitions	Number of false alarms eliminated	• Prioritized anomaly lists • Scoring reports from the IDA	Reduction of false alarms by over 75% while retaining all targets of interest
Specification of no-dig threshold	Probability of correct classification and number of false alarms at demonstrator operating point	• Demonstrator-specified threshold • Scoring reports from the IDA	Threshold specified by the demonstrator to achieve the criteria specified above
Minimize the number of anomalies that cannot be analyzed	Number of anomalies that must be classified as "Unable to Analyze"	• Demonstrator target parameters	Reliable target parameters can be estimated for over 90% of anomalies on each sensor's detection list.
Correct estimation of target parameters	Accuracy of estimated target parameters	• Demonstrator target parameters • Results of intrusive investigation	Total ONVMS ± 10% X, Y < 10 cm Z < 5 cm size ± 10%

3.1 Objective: maximize correct classification of munitions

The effectiveness of the technology for discrimination of munitions is maximizing correct classification of targets of interests from non-TOI with high (99.9%) confidence.

3.1.1 Metric

Identify all seeded and native TOI with high confidence using advanced EMI discrimination technologies. (The Program Office did not quantify "high confidence.") Our estimates were based on using the extracted total ONVMS as input to statistical classification algorithms and expert judgment. Every anomaly that was close to a TOI cluster in feature space was considered a possible TOI; the expert then inspected the corresponding total ONVMS curve for symmetry (manifested by equal secondary and tertiary ONVMS amplitudes) and signal-to-noise ratio.

3.1.2 Data requirements

We analyzed data from three instruments: MM, 2 × 2-3D TEMTADS, and MPV-II. For each sensor we identified custom training data sets (using not more than ~10 % of entire data). We requested the ground truth for the custom training data sets and used them to validate the models for each specific site and sensor. We generated dig-lists that were scored by IDA.

3.1.3 Success criteria evaluation and results

The objective was considered to be met if all seeded and native UXO items can be identified below an analyst-specified no-dig threshold.

3.1.4 Results

This objective was successfully met. All TOI, both seeded and native (including small fuzes and fuze parts), were identified with high confidence using the advanced EMI discrimination technology. Figure 9, Figure 10, Figure 20, and Figure 23 show the ROC curves obtained for MM data (by CH2M HILL and Parsons), for the 2 × 2 TEMATDS, and for the MPV. All TOI were classified correctly.

3.2 Objective: maximize correct classification of non-munitions

The technology aims to minimize the number of false negatives, i.e. maximize the correct classification of non-TOI.

3.2.1 Metric

We compared the number of non-TOI targets that can be left in ground with high confidence using the advanced EMI discrimination technology to the total number of false targets that would be present if the technology were absent.

3.2.2 Data requirements

This objective required prioritized anomaly lists, which our team generated independently for each sensor, and for its evaluation we needed scoring reports from IDA.

3.2.3 Success criteria evaluation and results

The objective was considered to have been met if the method eliminated at least 75% of targets that did not correspond to targets of interest in the discrimination step.

3.2.4 Results

This objective was successfully met. The advanced EMI discrimination technology was able to eliminate 86% , 81% , 76%, and 75% of non-TOI respectively for the CH2MHILL and Parsons MM analyses, the 2 × 2 TEMATDS data, and the MPV data. All TOI were classified correctly.

3.3 Objective: specify a no-dig threshold

This project aims to provide high classification confidence approach for UXO-site managers. One of the critical quantities for minimizing UXO residual risk and providing regulators with acceptable confidence is no-dig threshold specification.

3.3.1 Metric

We compared an analyst's no-dig threshold point to the point where 100% of munitions were correctly identified.

3.3.2 Data requirements

To meet this requirement we needed scoring reports from IDA.

3.3.3 Success criteria evaluation and results

The objective would be met if a sensor-specific dig list placed all the TOI before the no-dig point and if additional digs (false positives) were requested after all TOI were identified correctly.

3.3.4 Results

This objective was successfully met for all data sets. See Figure 9, Figure 10, Figure 20, and Figure 23.

3.4 Objective: minimize the number of anomalies that cannot be analyzed

Some anomalies may not be classified either because of the data are not sufficiently informative—the sensor physically cannot provide the data to support classification for a given target at a given depth—or because the data processing was inadequate. The former is a measure of instrument performance for all anomalies for which all data analysts converge. The latter is a measure of our data analysis quality where our target diagnostic differs from that made by other analysts.

3.4.1 Metric

The metric for this objective is the number of anomalies that cannot be analyzed by our method, and the intersection of all anomaly lists among all analysts.

3.4.2 Data requirements

Each analyst submitted their anomaly list. IDA scored all lists and returned a list of anomalies that could not be analyzed by any analyst ("cannot analyze" or "failed classification").

3.4.3 Success criteria evaluation and results

The objective was met if at least 95% of the selected anomalies that verify the aforementioned depth requirement could be analyzed.

3.4.4 Results

This objective was successfully met. All four data sets for all anomalies were analyzed. Not a single anomaly was ranked as "cannot analyze."

3.5 Objective: correct estimation of target parameters

The combined ONVMS-DE algorithm provides intrinsic and extrinsic parameters for the different targets. The intrinsic parameters were used for classification, while the extrinsic parameters (i.e., the target locations) were utilized for residual risk assessment.

3.5.1 Metric

The classification results entirely depend on how accurately these parameters are estimated.

3.5.2 Data requirements

To achieve this objective we inverted and tabulated the intrinsic and extrinsic parameters for all targets. To validate extracted extrinsic parameters we needed results of intrusive investigations.

3.5.3 Success criteria evaluation and results

The objective was met if the targets intrinsic parameters varied within $\pm$10%, the extracted *x-y* location within $\pm$10 cm, and the depth within $\pm$5 cm.

3.5.4 Results

The clustering seen in the targets' inverted intrinsic indicates that this objective was successfully met for all data. To verify results we compared the estimated depths to actual depths for all emplaced and side specific targets. Figure 24 and Figure 25 show (for the MetalMapper and portable, respectively) the distribution of depth errors (defined here by as $| Z^{estimated} - Z^{data} |$) The MetalMapper discrepancies have a mean of 4.07 cm and a standard deviation of 5.03 cm; for 2x2 TEMTADS the mean is 4.97 cm and the standard deviation is 4.35 cm, and for MPV-II the mean is

4.62 cm and the standard deviation is 4.2 cm. The errors in horizontal locations obey similar distributions. Thus the agreement between inverted and actual values were good for all instruments.

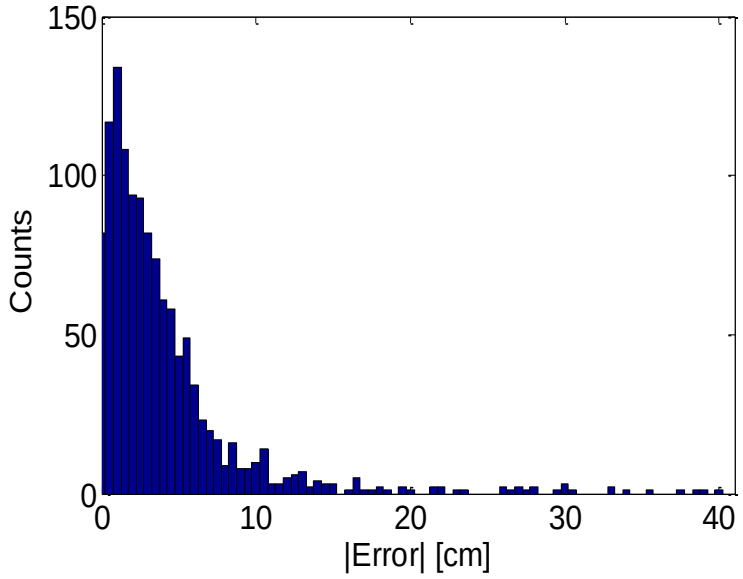

Figure 24 Histogram of depth errors (defined as $| Z^{estimated} - Z^{data} |$) for the set of Camp Beale CH2NHILL MetalMapper anomalies. The distribution shown has a mean of 4.07 cm and a standard deviation of 5.03 cm. There is good agreement between the estimates and the ground truth.

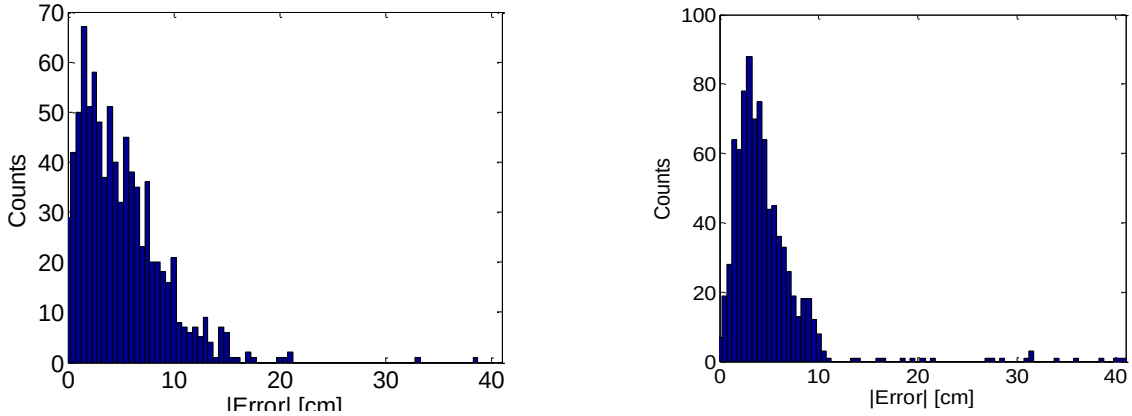

Figure 25 Histogram of depth errors (defined as $| Z^{estimated} - Z^{data} |$) for the set of Camp Beale portable instruments anomalies. The depth errors distributions are shown for 2x2 TEMTADS (left) and MPV-II (right) instruments , which have means of 4.97 cm and 4.62 cm, and standard deviations of 4.35 and 4.2 cm, respectively.

4 TEST DESIGN

The only required test at the Camp Beale site entailed collecting target characterization training data: Using a calibration pit, the data-collection team made a series of static measurements of example targets at several depths and attitudes in order to cross-check models, confirm Tx and Rx polarity for the sensors, and characterizer the so-called *Library* targets.

4.1 Site preparation

N/A.

4.2 Demonstration schedule

	Preparation Calibration	Blind data set			Post-survey analysis		
Tasks and demonstration stages	**Aug2011**	**Sep -11**	**Oct-11**	**Nov -11**	**Dec -11**	**Jan -12**	**Feb -12**
1. Invert all calibration data sets	x						
2. Invert 2 × 2-3D TEMTADS data		x					
3. Invert MM data sets		x					
4. Invert MPV-II data		x					
5. Build custom training data sets and request ground truth for TEMTADS			x				
6. Build custom training data sets and request ground truth for MM			x				
7. Build custom training data sets and request ground truth for MPV-II			x				
8. Redefine the MM classifier and request more training data if necessary			x				
9. Redefine the 2 × 2-3D TEMTADS target classifier and request additional training data if necessary			x				
10. Redefine the MPV-II target classifier and request addition training data if necessary			x				
11. Generate MM dig list and submit to IDA				x			
12. Generate TEMTADS dig list and submit to IDA				x			
13. Generate MPV-II dig list and submit to IDA				x			
14. Conduct retrospective analysis if needed					x	x	
REPORTING:							
15. Draft demo plan	X						
16. Final demo plan	X						
17. Draft demonstration report						x	
18. Final demonstration report							x

Figure 26. Gantt chart showing a detailed schedule of the activities conducted at Camp Beale.

5 DATA ANALYSIS PLAN

We analyzed all cued data for the MetalMapper, 2 × 2-3D TEMTADS, and MPV-II sensors and produced prioritized dig lists for independent scoring.

5.1 Extracting target locations

Target locations were determined relative to the sensor coordinate system using the differential evolution algorithm. Objects responses were modeled with ONVMS. This combined ONVMS-DE algorithm was run for single- and multi-target cases and provided target locations.

5.2 Extracting target intrinsic parameters

5.2.1 Single targets

The combined ONVMS-DE algorithm yields the targets' intrinsic total ONVMS, which we used for classification. The total ONVMS contains three moments, $M_{xx}(t)$, $M_{yy}(t)$, and $M_{zz}(t)$, along the primary axes in the target's own reference frame. These moments are similar to simple dipole moment components but carry more information, accounting for the targets' inherent heterogeneities. The ONVMS-DE algorithm outputs the time-decay curves of the target's total ONVMS tensor $M_{ij}(t_k)$. The next step is to determine the time decay of the primary components of the total ONVMS in the target's reference frame. While this can be done by standard diagonalization (i.e., finding $M(t_k) = V(t_k)D(t_k)V^T(t_k)$, where $V(t_k)$ contains the eigenvectors of $M(t_k)$, it is more convenient to perform a joint diagonalization, $M(t_k) = VD(t_k)V^T$, where now the eigenvectors are shared by all time channels; this allows us to extract more reliable total ONVMS values and reduce uncertainty. The resulting temporal decay of the total principal ONVMS for Camp Butner anomalies is illustrated in Figure 7 and Figure 8 for the MetalMapper, in Figure 17, Figure 18, and Figure 19 for the 2 × 2 TEMTADS, and in Figure 21 and Figure 22 for the MPV-II.

5.2.2 Multi-target cases

A similar approach is carried out if more than one subsurface target is expected. The DE algorithm now searches for the locations and the total ONVMS of several objects. Such multi-target inversion is crucial in the field for cases in which a signal from a UXO is mixed with EMI signals from nearby clutter (see Anomaly 758 in Figure 14). Out two-target inversion code yields three sets of location and total ONVMS estimates: one for Target 1, one for Target 2, and a combined estimate with Targets 1 and 2 represented by a single object. (In the case of 3-target inversion, seven sets of data are expected: only Target 1, only Target 2, only Target 3, Targets 1 and 2 as a single object, Targets 2 and 3 as a single object, Targets 1 and 3 as a single object, and all three targets acting as a single object. In the general case of *n* targets one expects $n(n-1)+1$ sets of ONVMS curves).

5.3 Selection of intrinsic parameters for classification

Most UXO are bodies of revolution, and thus the two secondary polarizability elements are degenerate. However, live-site UXO discrimination studies have repeatedly shown that this symmetry can be compromised due to low SNR, especially for small or deep targets. A good classification of object features can then be obtained by using only the principal component of the total ONVMS (M_{zz}). Furthermore, to limit the number of relevant features for use in classification we will extract parameters exclusively from the main polarizability $M_{zz}(t)$, both to represent size $M_{zz}(t_1)$ and wall thickness $M_{zz}(t_n) / M_{zz}(t_1)$. The interested reader is referred to Section 2.4.

5.4 Training

Our classification approach is based on custom training data. At the first stage of the process we used a semi-supervised clustering technique for indentifying potential site-specific TOI. Below are the basic steps performed during training data selection; for more details regarding each specific sensor see Section 2.4.

(a) The targets intrinsic features ($M_{zz}(t_1)$, $M_{zz}(t_n) / M_{zz}(t_1)$) were selected from the extracted total ONVMS; *n* was chosen based on feature separation. EMI data sets of all anomalies, corresponding to single- and multi-object inversions, were produced.
(b) Initial clustering was performed. The ground truth was requested for all targets whose features were located closest to the corresponding cluster centroid and had TOI-like ONVMS features.
(c) Clusters containing at least one TOI were identified, and a smaller domain was selected within the feature space for further interrogation.
(d) Additional clustering was performed within the selected domain, and those targets with features closest to the corresponding cluster centroids were probed for ground truth. The clusters with at least one identified UXO were marked as *suspicious*. The total ONVMS curves were inspected within the selected domain
(e) All targets whose features (based on multi-object inversion and library matching) fell inside any of the *suspicious* clusters were used to train the statistical classifier and the library-matching procedure.

5.5 Classification

(f) Probability density functions were extracted for single- and multi-target scenarios.
(g) All of the unknown targets were scored based on the probability density functions.
(h) Dig lists were produced for both single- and multi-object cases and compared to each other to find similarities and differences.
(i) All items were further analyzed using library matching, and all total ONVMS time-decay curves were inspected visually.

(j) A set of anomalies were identified and additional training data sets were requested. The new information was incorporated into the Gaussian mixture model and all items were re-scored.
(k) Based on the previous steps a classification threshold was selected and a final dig list was produced.

5.6 Decision memo

The algorithms used to select training data and to perform inversion and classification for the Camp Beale test are described in Section 2.4. Using the inversion, clustering, classification and data-requesting procedures outlined above we produced a ranked anomaly list formatted as specified by IDA [29].

6 COST ASSESSMENT

Time and resources were tracked for each task to assess the cost of deploying the technology at future live sites. Note that some of the costs might decrease as the technology matures and survey procedures get formalized. A cost model, that spent by non-experts during Camp Beale targets classification using the advanced models, is summarized in Table 2.

Table 2: Cost model for advanced EMI model demonstration at the former Camp Beale

Cost Category	Description	Cost
Preprocessing	Time required to perform eigenvalue extraction, check data quality, and estimate the number of potential anomalies	0.25 min/anomaly
Parameter extraction	Time required to run code and extract target feature parameters	0.25 min/anomaly
Classifier training	Time required to optimize classifier design and train	1 min/anomaly
Classification and construction of a ranked anomaly list	Time required to classify anomalies in the test set and construct the ranked anomaly list	1.5 min/anomaly
	Total	3 min/anomaly

7 MANAGEMENT AND STAFFING

Figure 27 is the organization chart for the personnel involved in the demonstration. Their responsibilities are as follows:

1. Fridon Shubitidze – Principal Investigator. Responsible for MPV-II and CH2MHILL MM data inversion and classification.
2. Irma Shamatava – Sky Research Geophysicist. Responsible for 2 × 2-3D TEMTADS data inversion and classification.
3. Joe Keranen and Jon Miller – Sky Research Geophysicists. Responsible for Parsons MM data inversion and classification.

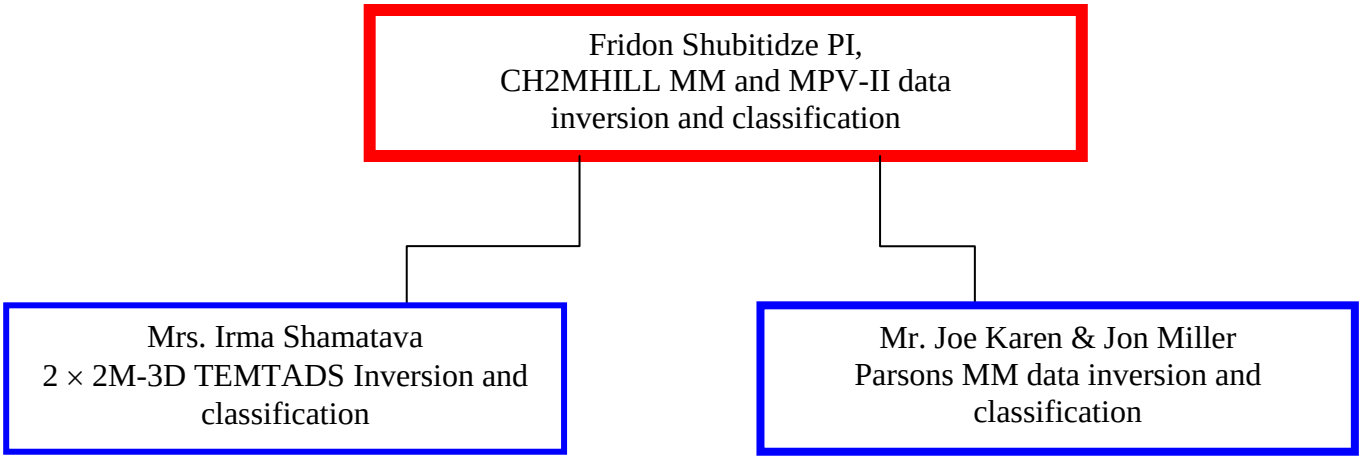

Figure 27: Project management hierarchy.

8 REFERENCES

[1] "ESTCP Munitions Response, Live Site Demonstrations, former Camp Beale, CA, April 2011, Draft 4," dated June 2, 2011

[2] ESTCP, "2009 ESTCP UXO Classification Study, San Luis Obispo, CA," Environmental Security Technology Certification Program, Arlington, VA, Demonstration Plan, April 2009.

[3] M. Prouty, "Detection and Classification with the MetalMapper™ at Former Camp San Luis Obispo," ESTCP Project No. MM-0603, Geometrics, Inc. July 2009.

[4] I. Shamatava, F. Shubitidze, B. E. Barrowes, J. P. Fernández, K. A. O'Neill, and A. Bijamov, "Live-site UXO classification studies using advanced EMI and statistical models," *Proceedings of SPIE* vol. 8017, 8017-08, (2011).

[5] I. Shamatava, F. Shubitidze, J. P. Fernández, B. E. Barrowes, K. A. O'Neill, and T. M. Grzegorczyk, "SLO blind data set inversion and classification using physically complete models," *Proceedings of SPIE,* vol. 7664, 7664-03 (2010).

[6] F. Shubitidze et al., "Camp Butner UXO Data Inversion and Classification Using Advanced EMI Models," SERDP-ESTCP Partners 2010.

[7] F. Shubitidze, B. E. Barrowes, I. Shamatava, J. P. Fernández, T. M. Grzegorczyk, K. O'Neill, and A. Bijamov, "Advanced UXO discrimination: resolving multiple targets and overlapping EMI signals," in R. S. Harmon, J. H. Holloway, and J. T. Broach, eds., *Detection and Sensing of Mines, Explosive Objects, and Obscured Targets XVI, Proceedings of SPIE* vol. 8017, 8017-09, 2011.

[8] A. Paski et al., "Former Camp Butner Site Description and EM61 Data Collection and Analysis," SERDP-ESTCP Partners 2010.

[9] L. Pasion et al., "UXO Discrimination Using Full Coverage and Cued Interrogation Data Sets at Camp Butner, NC," SERDP-ESTCP Partners 2010.

[10] D. Keiswetter et al., "SAIC Data Analysis of Data Acquired at Camp Butner," SERDP-ESTCP Partners 2010.

[11] S. Billings et al., "Processing and Discrimination Strategies for Next-Generation EMI Sensor Data," SERDP-ESTCP Partners 2010.

[12] D. Keiswetter et al., "EM61 and Magnetic Sensors: Application and Performance Summary at Camp SLO," SERDP-ESTCP Partners 2010.

[13] F. Shubitidze, D. Karkashadze, J. P. Fernández, B. E. Barrowes, K. O'Neill, T. M. Grzegorczyk, and I. Shamatava, "Applying a Volume Dipole Distribution Model to Next-Generation Sensor Data for Multi-Object Data Inversion and Discrimination," *Proceedings of SPIE,* vol. 7664, 2010.

[14] F. Shubitidze et al., "A complex approach to UXO discrimination: Combining advanced EMI forward models and statistical signal processing," SERDP MR-1572 Final Report, January 2012.

[15] J.-F. Cardoso and A. Souloumiac. "Jacobi angles for simultaneous diagonalization," *SIAM J. Mat. Anal. Appl.*, vol. 17, pp. 161–164, 1996.

[16] L. Beran and D.W. Oldenburg, "Selecting a Discrimination Algorithm for Unexploded Ordnance Remediation," *IEEE Transactions on Geoscience and Remote Sensing*, vol. 46, pp. 2547–2557, 2008.

[17] J. Byrnes, Ed., *Unexploded Ordnance Detection and Mitigation*, ser. NATO Science for Peace and Security Series B: Physics and Biophysics. Dordrecht: Springer Netherlands, 2009.

[18] Y. Zhang, L. Collins, H. Yu, C. E. Baum, and L. Carin, 2003, "Sensing of Unexploded Ordnance with Magnetometer and Induction Data: Theory and Signal Processing," *IEEE Trans. Geosci. Remote Sensing*, vol. 41, pp. 1005–1015, 2003

[19] S. D. Billings, "Discrimination and classification of buried unexploded ordnance using magnetometry," *IEEE Transactions of Geoscience and Remote Sensing*, vol. 42, pp. 1241–1251, 2004

[20] Carin, L., Zhang, Y. and Liao, X., 2004, Detection of Buried UXO via Active Selection of Labeled Data: Presentation at The UXO Forum 2004.

[21] R. E. Grimm, "Triaxial modeling and target classification of multi-channel, multicomponent EM data for UXO discrimination," *Journal of Environmental and Engineering Geophysics*, vol. 8, pp. 239–250, 2003.

[22] J. P. Fernández, F. Shubitidze, I. Shamatava , B. Barrowes, and K. O'Neill, "Realistic subsurface anomaly discrimination using electromagnetic induction and an SVM classifier", Journal in Advanced Signal Processing, 2010.

[23] Hart, S.J. et al. (2001) Using Physics Based Modeler Outputs to Train Probabilistic Neural Networks for Unexploded Ordnance (UXO) Classification in Magnetometry Surveys. *IEEE Trans. Geosci. Remote Sensing* 39, 797-804.

[24] P. Comon, "Independent component analysis, a new concept?" *Signal Processing*, vol. 36, pp. 287–314, 1994.

[25] Dempster, A., Laird, N., and Rubin, D. (1977). Maximum likelihood from incomplete data via the EM algorithm. *Journal of the Royal Statistical Society, Series B*,39(1):1–38.

[26] R. Storn, and K. Price, "Differential evolution: a simple and efficient adaptive scheme for global optimization over continuous spaces," *Journal of Global Optimization*, vol. 11, pp. 341–359, 1997.

[27] R. Storn, "System design by constant adaptation and differential evolution," *IEEE Trans. Evol. Comput.*, vol. 3, pp. 22–34, 1999.

[28] F. Shubitidze, K. O'Neill, B. E. Barrowes, I. Shamatava, J. P. Fernández, K. Sun, and K. D. Paulsen, "Application of the normalized surface magnetic charge model to UXO discrimination in cases with overlapping signals," *Journal of Applied Geophysics*, vol. 61, pp. 292–303, 2007.

[29] S. Cazares and M. Tuley, "UXO Classification Study: Scoring Memorandum for the former Camp San Luis Obispo, CA," Institute for Defense Analyses, 13 March 2009

9 APPENDICES

9.1 Appendix A: Health and Safety Plan (HASP)

As this effort does not involve field data collection, no HASP is required.

9.2 Appendix B: Points of Contact

Points of contact (POCs) involved in the demonstration and their contact information are presented in Table 3.

Table 3: Points of Contact for the advanced EMI models demonstration.

POINT OF CONTACT Name	ORGANIZATION Name Address	Phone Fax E-mail	Role in Project
Dr. Fridon Shubitidze	Sky Research Inc.	Tel: 603 643 2876 Fax: 603-643-5161 fridon.shubitidze@skyresearch.com	PI
Erik Russell	Sky Research Inc. 3 School House Lane, Etna, NH, 03750, USA	Tel: 541-552-5197 Fax: 603-643-5161 Erik.Russell@skyresearch.com	Project Coordination
Dr. Herb Nelson	ESTCP Program Office ESTCP Office 901 North Stuart Street, Suite 303 Arlington, VA 22203-1821	Tel: 703-696-8726 Herbert.Nelson@osd.mil	ESTCP Munitions Management Program Manager

9.3 Appendix C: DATA Pre-processing and formatting for ONVMS code

The next generation EMI data are provided in a comma-delimited format. These data are pre-processed using the JD algorithm and converted to a new ASCII format that the ONVMS code can accept. The following Matlab script creates PNG figures of eigenvalues vs. time from the provided CSV files and converts them to the ONVMS-compatible ASCII format.

```
function TRASFER_CSV_to_MM_ONVMS()
clear all
% User must specify folder for MM CSV files
    file_dir1='C:\CAMP_BEALE\MM_ANOMALIES\CH2MHILL\test';
    DATA_transfer(file_dir1)

end

function DATA_transfer(file_dir1)
for ifile=1:1
File_numb=int2str(ifile);
file_dir=strcat(file_dir1); %,File_numb);
D_folder=dir(file_dir);
Nfille=size(D_folder);
if (Nfille<1)
else
File_ty={D_folder.name};
for irun=3:length(File_ty)
File_name1=File_ty{irun};
A_logic=File_name1(length(File_name1)-2:length(File_name1));
B_logic='csv';
if A_logic==B_logic;
 File_name = strcat(file_dir,'\',File_name1);
 Output_file_name=strcat(file_dir,'\',File_name1(1:length(File_name1)-4),'_data_pr.flt');
Signaly=csvread(File_name,2,25);
mn=0;
for ir=1:7
for itx=1:3
for ic=1:3
mn=mn+1;
Hfld(ir,itx,ic,:)=Signaly(:,mn+4);
end
end
end
%%%%%%%%%%%%%%%%%%%%%%%%%%%%


Ns_param=length(Signaly(:,4));
TEMTADS_time=Signaly(10:Ns_param,1);
Nt_param=length(TEMTADS_time);

[Dt]=Joint_diagonal(Nt_param,Ns_param, Hfld);

h2=figure(101);
for i=1:21;
loglog(TEMTADS_time(:), abs(Dt(i,:)),'b','LineWidth', 3); hold on;
end

File_id=strcat('Case-',File_name1(length(File_name1)-4-4:length(File_name1)-4));
File_name_figure1=strcat('Case_',File_name1(length(File_name1)-4-4:length(File_name1)-4));

set(h2,'ReSize','on')
%set(h2,'Position',[580 324 880 574])
axis([(TEMTADS_time(1)) max(TEMTADS_time) 1e-6 1e5])

hsc=gca; set(hsc,'FontSize', 16);
xlabel('Time [sec]', 'FontSize', 16)
ylabel('Eigenvalues [Arb]', 'FontSize', 16);
%grid on
```

```
legend (File_id)
print( gcf, '-dpng', File_name_figure1 )
hold off

%%%%%%%%%%%%%%%%%%%%%%%%%%%%%%%%%%%%555555

Rx_cor(1:3,1:7)=0.15;
Rx_cor(1:2,1)=0.39;
Rx_cor(1,2)=-0.26;
Rx_cor(2,2)=0.26;

Rx_cor(1:2,3)=0.13;
Rx_cor(1:2,4)=0.0;
Rx_cor(1:2,5)=-0.13;
Rx_cor(1,6)=0.26;
Rx_cor(2,6)=-0.26;
Rx_cor(1:2,7)=-0.39;

Tx_cor(1:3,1:3)=0.0;
Tx_cor(3,1)=0.15;
Tx_cor(3,2)=0.56+0.15;
Tx_cor(3,3)=0.56+0.15;
Angl_fi(1)=0.0;
Angl_te(1)=0.0;

Angl_fi(2)=pi/2;
Angl_te(2)=pi/2;

Angl_fi(3)=0.0;
Angl_te(3)=pi/2;

fi_ant=0;
teta_ant=pi/4;


A_ant(1,1)=cos(teta_ant)*cos(fi_ant);
A_ant(1,2)=-sin(fi_ant);
A_ant(1,3)=sin(teta_ant)*cos(fi_ant);

A_ant(2,1)=cos(teta_ant)*sin(fi_ant);
A_ant(2,2)=cos(fi_ant);
A_ant(2,3)=sin(teta_ant)*sin(fi_ant);

A_ant(3,1)=-sin(teta_ant);
A_ant(3,2)=0.0;
A_ant(3,3)=cos(teta_ant);



frmt1=' %12.5e %12.5e %12.5e %12.5e %12.5e';
frmt2=' %12.5e %12.5e %12.5e %12.5e %12.5e\n';
frmttime=repmat(frmt1,1,9);
frmt=repmat(frmt1,1,11);
frmt=strcat(frmt,frmt2);
fid=fopen('MM_Time.txt','w');
fprintf(fid,frmttime,Signaly(6:50,1));
fclose(fid);
 fid=fopen(Output_file_name,'w');
 for ir=1:7
for itx=1:3

fi_ant=Angl_fi(itx);
teta_ant=Angl_te(itx);


A_ant(1,1)=cos(teta_ant)*cos(fi_ant);
A_ant(1,2)=-sin(fi_ant);
A_ant(1,3)=sin(teta_ant)*cos(fi_ant);

A_ant(2,1)=cos(teta_ant)*sin(fi_ant);
A_ant(2,2)=cos(fi_ant);
```

```
A_ant(2,3)=sin(teta_ant)*sin(fi_ant);

A_ant(3,1)=-sin(teta_ant);
A_ant(3,2)=0.0;
A_ant(3,3)=cos(teta_ant);


for ic=1:3
mn=mn+1;
Y_mat(mn,1:45)=Hfld(ir,itx,ic,6:50);
fprintf(fid,frmt,Tx_cor(1:3,itx),Rx_cor(1:3,ir),A_ant(1,1:3),A_ant(2,1:3),A_ant(3,1:3),Y_mat(mn,1
:45));

end
end
end

pause
fclose(fid);


end
end
end

end
end
```

9.4 Run ONVMS code

After being preprocessed and converted to the ONVMS-compatible format the data are inverted using the combined ONVMS-DE code (‘ONVMS_MM.exe’). A Matlab script that runs the ONVMS-DE code is provided here. The user must specify the locations of the converted ONVMS files and the output files and provide the number of potential targets and the boundaries of the search volume.

```
function run_inversion_code ()
clear all

%An user must provide following variables

Input_files_folder='C:\CAMP_BEALE\MM_ANOMALIES\PARSON\flt_files'; % User must provide
Output_files_folder_uxo='C:\CAMP_BEALE\MM_ANOMALIES\PARSON\Inversion_parson\UXO\';  %  User  must
provide
Output_files_folder_de='C:\CAMP_BEALE\MM_ANOMALIES\PARSON\Inversion_parson\TXT\';  %  User  must
provide
Output_files_folder_dat='C:\CAMP_BEALE\MM_ANOMALIES\PARSON\Inversion_parson\DAT\';  %  User  must
provide

fid=fopen('MAS_PARAM_ENTRY.inp','w');
  Ntargets=1;   %%% Number of Targets;
  Number_iter=100;  %%% Number of Iterations for DE algorithm;
  Xmin=-1.5;   %%% X minimum value for a search volume under the sensor
  Xmax=1.5;   %%% X maximum .....................................
  Ymin=-1.5;   %%% Y minimum .....................................
  Ymax=1.5;   %%% Y maximum .....................................
  Zmin=-1.2;   %%% Z minimum .....................................
  Zmax=0.02;   %%% Z maximum .....................................


fprintf(fid, '%6i %6i\n', Ntargets,Number_iter);
fprintf(fid, '%10.4e %10.4e\n',Xmin, Xmax);
fprintf(fid, '%10.4e %10.4e\n',Ymin, Ymax);
fprintf(fid, '%10.4e %10.4e\n',Zmin, Zmax);

fclose (fid)
File_prefix=int2str(Ntargets);
run_ONVMS_MM(File_prefix,   Input_files_folder,Output_files_folder_uxo,   Output_files_folder_de,
Output_files_folder_dat);
end


function          run_ONVMS_MM(File_prefix,          Input_files_folder,Output_files_folder_uxo,
Output_files_folder_de, Output_files_folder_dat)

for ifile=1:1

File_numb=int2str(ifile);
file_dir=Input_files_folder;
D_folder=dir(file_dir);
Nfille=size(D_folder);
if (Nfille<1)
else

File_test={D_folder.name};

for irun=3:length(File_test)

File_name1=File_test{irun};
A_logic=File_name1(length(File_name1)-2:length(File_name1));
B_logic='flt';

if A_logic==B_logic;
 File_name = strcat(file_dir,'\',File_name1);
Input_data_file_name =strcat(file_dir,'\',File_name1(1:length(File_name1)-4),'.flt');
```

```
  DE_Outputfile=strcat(Output_files_folder_de,'Case_iter_',File_name1(1:length(File_name1)-
4),'_',File_prefix,'.txt');
Output_ONVMS_file=strcat(Output_files_folder_uxo,'Case_',File_name1(1:length(File_name1)-
4),'_',File_prefix,'.uxo');
Output_Data_Model_file=strcat(Output_files_folder_dat,'Case_',File_name1(1:length(File_name1)-
4),'_',File_prefix,'.dat');



fid=fopen('Input_files.inp','w');

fprintf(fid, '%s\n', Input_data_file_name);
fprintf(fid, '%s\n',Output_Data_Model_file);
fprintf(fid, '%s\n', Output_ONVMS_file);

fclose(fid);

fid=fopen('DE.inp','w');
 fprintf(fid, '%s\n', DE_Outputfile);
 fclose(fid);

system('ONVMS_MM.exe');
 fclose('all');
end
end
end


end
end
```

9.5 Generate Custom Training Data list

The combined ONVMS-DE algorithm generates the total ONVMS for each anomaly. Targets are clustered using their size and decay parameters, and a custom training data list is created. The following Matlab script clusters the anomalies and produces the lists. The user must provide the inverted total ONVMS.

```
function Custom_Ground_truth

Time_channel=37;
Input_mat_file='CH2MHILL_1trgclusterring.mat';
Percent=8; % <-------- how many percent of the total number of anomalies
Output_csv_file='CH2MHILL_GrdTr.csv';
TargClust_GrdTruthReq(Time_channel,Percent, Input_mat_file,Output_csv_file )
 end

 function [Dat]=TargClust_GrdTruthReq(Time_channel,Percent, Input_mat_file,Output_csv_file )

load (Input_mat_file);
 Nch = size(RatioY,2);
 for iTime=Time_channel:Time_channel%2:Nch
 %% Just Plot:
 X(1:1490,1) = log10(RatioX(1,1:1490));
 X(1:1490,2) = log10(RatioY(1:1490,iTime));
 figure(2*Time_channel-1);
 plot(X(:,1),X(:,2),'.r')
 title(sprintf('%d',iTime));
 %% Find clusters:
 nClusters = round(Percent/100*size(X,1)) % <-------- how many clusters, compared to the number
of anomalies
% dstfunc = 'mahalanobis';
% lnkfunc = 'weighted';
 dstfunc = 'euclidean';
 lnkfunc = 'ward';
 cID = clusterdata(X,'maxclust',nClusters,'distance',dstfunc,'linkage',lnkfunc);

 figure(2*Time_channel);
 d9=scatter(X(:,1),X(:,2),82,cID,'filled'); colormap lines; hold on;

 title(sprintf('%d',iTime));

 %% Find centers for training:
 trn1 = zeros(nClusters,1);
 for ic=1:nClusters
 IND = find(cID==ic);
 [mmm,iii] = min( sum( ( X(IND,:)-repmat(mean(X(IND,:),1),length(IND),1) ).^2, 2) );
 trn1(ic) = IND(iii);

 figure(2*Time_channel);
 plot(X(trn1(ic),1),X(trn1(ic),2),'ok','MarkerSize',15, 'LineWidth', 2); hold on;
 end
 xlabel ('Log_1_0(M_z_z(t_1))', 'FontSize',16);
 ylabel ('Log_1_0(M_z_z(t_3_7)/M_z_z(t_1))', 'FontSize',16);

 htt=gca;
 set(htt,'FontSize', 16)

 fid = fopen('Temp_mat.dat','w');
 fprintf(fid,'%d\n',trn1');
 fclose(fid);

 figure(2*Time_channel); hold off;
 end
Dat=load('Temp_mat.dat');
csvwrite(Output_csv_file,sort(Dat));
end
```